Journal of
Low Power Electronics and Applications

MDPI

Article

Evaluation of Residential Photovoltaic Systems for Charging Electric Vehicles Using a Hardware-in-the-Loop Technique

Edgar López-Molina [1], Víctor Sámano-Ortega [2,*], Alejandro Israel Barranco-Gutiérrez [3], Alejandra Ramírez-Segovia [4], Ricardo Lozoya-Ponce [5] and Juan Martínez-Nolasco [2,*]

[1] Doctorado en Ciencias de la Ingeniería, Tecnológico Nacional de México/IT de Celaya, Antonio García Cubas 600, Celaya 38010, Mexico; d2503100@itcelaya.edu.mx
[2] Departamento de Ingeniería Mecatrónica, Tecnológico Nacional de México/IT de Celaya, Antonio GarcíaCubas 600, Celaya 38010, Mexico
[3] Departamento de Ingeniería Electrónica, Tecnológico Nacional de México/IT de Celaya, Antonio GarcíaCubas 600, Celaya 38010, Mexico; israel.barranco@itcelaya.edu.mx
[4] Departamento de Ciencias Básicas, Tecnológico Nacional de México/IT de Celaya, Antonio García Cubas 600, Celaya 38010, Mexico; alejandra.ramirez@itcelaya.edu.mx
[5] División de Estudios de Posgrado e Investigación, Tecnológico Nacional de México/IT de Chihuahua, Ave. Tecnológico 2909, Chihuahua 31200, Mexico; ricardo.lp@chihuahua.tecnm.mx
* Correspondence: victor.samano@itcelaya.edu.mx (V.S.-O.); juan.martinez@itcelaya.edu.mx (J.M.-N.)

Abstract

This study analyzes the energy consumption, operating costs, and associated CO_2 emissions of electric vehicle (EV) charging under different residential photovoltaic system (RPVS) configurations using a Hardware-in-the-Loop (HIL) platform. Three charging scenarios were evaluated: (i) EV charging supplied exclusively by the main grid (MG); (ii) EV charging supplied by an off-grid RPVS; and (iii) EV charging supplied by an interconnected RPVS supported by the MG. To perform the experimental evaluation, an HIL platform integrating a microgrid (μG) and an EV emulator was developed. The EV emulator was configured using the parameters of a Tesla Model S battery pack based on 18,650 lithium-ion cells. The embedded μG architecture was reprogrammed to include an RPVS, a battery bank (BB), an AC bus, and the capability to operate either autonomously or interconnected with the MG. Energy balance within the μG was managed through an Energy Management System (EMS) designed to maximize the utilization of photovoltaic energy. The experimental results showed that Scenario 1 Level 1 required 100.344 kWh, while Scenario 1 Level 2 required 105.982 kWh. In Scenario 2, energy consumption was 101.856 kWh, and Scenario 3 required 104.4 kWh. Based on these data, the estimated monthly energy consumption, CO_2 emissions, and costs were as follows: for Scenario 1, 251.23 kWh, 111.54 kg CO_2, and 1692.25 MXN; for Scenario 2, 251.23 kWh, 12.53 kg CO_2, and 262.28 MXN; and for Scenario 3, an exportation of 1007.45 kWh to the MG, 174.36 kg CO_2, and 1340.81 MXN. These results provide technical and environmental evidence supporting the feasibility of RPVS for EV charging and highlight the importance of renewable energy-based solutions for sustainable electric mobility. The proposed HIL-based methodology offers a reliable framework for assessing the technical, economic, and environmental impact of RPVS integrated with EV charging infrastructure.

Keywords: residential photovoltaic systems; electric vehicles; Hardware-in-the-Loop; microgrid; main grid

Academic Editors: Bingang Xu and Yujue Yang

Received: 16 October 2026
Revised: 3 November 2026
Accepted: 9 November 2026
Published: 11 November 2026

Copyright: © 2026 by the authors. Licensee MDPI, Basel, Switzerland. This article is an open access article distributed under the terms and conditions of the Creative Commons Attribution (CC BY) license.

1. Introduction

Greenhouse gas (GHG) emissions represent one of the most critical global challenges, contributing significantly to climate change and global warming. In response, international regulatory frameworks such as the Kyoto Protocol have required industrialized countries to limit, monitor, and periodically report their GHG emissions [1]. Subsequently, the Paris Agreement was adopted under the framework of the United Nations Climate Change Conference (COP), establishing ambitious long-term objectives to substantially reduce GHG emissions and maintain the increase in global average temperature well below 2 °C above pre-industrial levels, while pursuing efforts to limit it to 1.5 °C [2]. Furthermore, the agreement promotes the periodic review of national commitments every five years and encourages financial support for developing countries to strengthen climate adaptation and resilience capabilities [2].

Globally, the contribution of GHG emissions varies across regions; however, electricity generation, heating, and transportation remain the major emission sources within the energy sector [3,4]. In Mexico, approximately 85% of the energy consumed by the industrial and transportation sectors is still derived from fossil fuels. In response to this challenge, four energy scenarios have been projected through 2050. While the Business-as-Usual (BAU) scenario maintains the current energy structure, the Green Growth, Energy for a Decent Life, and Just and Sustainable Transition scenarios seek to satisfy national energy demand while significantly reducing GHG emissions. These alternative pathways converge on the urgent need to decrease dependence on fossil fuels and accelerate the decarbonization of the transportation sector through the adoption of cleaner and more sustainable energy sources [5].

Electric vehicles (EVs) have emerged as a key technology for mitigating GHG emissions in the transportation sector. However, their large-scale adoption may become counterproductive if the electricity used for charging is primarily generated from fossil fuels or if the increased charging demand compromises the stability of the main grid (MG) [6]. Currently, conductive (wired) charging remains the dominant method for EV battery replenishment, either through dedicated charging stations or residential charging equipment. Nevertheless, the charging process requires considerable amounts of electrical energy and may extend from several minutes to several hours depending on the charging level and battery capacity.

To address these challenges, advanced energy management strategies based on bidirectional power converters have been developed, enabling EV integration with different energy systems. These technologies include Vehicle-to-Grid (V2G), where EV batteries operate as distributed energy storage systems (ESSs) capable of supplying energy back to the grid; Vehicle-to-Home (V2H), in which EVs provide electricity to residential loads; Vehicle-to-Vehicle (V2V), which facilitates energy or information exchange between vehicles; and the broader Vehicle-to-Everything (V2X) paradigm, integrating bidirectional energy transfer and real-time data exchange among interconnected systems [7].

Within this framework, the integration of distributed energy resources (DERs) plays a fundamental role in reducing the environmental impact of EV charging. Among the available renewable energy technologies, solar photovoltaic (PV) systems have gained particular attention due to their widespread availability, decreasing installation costs, technological maturity, and suitability for residential applications [8,9].

Several studies have investigated the integration of renewable energy sources (RESs) for EV charging, with particular emphasis on PV energy systems [10]. For example, comprehensive simulation frameworks have been developed to analyze the entire energy flow, from electricity generation by PV modules to energy consumption by the vehicle powertrain. In the field of extended-range EVs, the integration of solar modules into vehicle structures has been proposed to increase driving autonomy through advanced

https://doi.org/10.3390/jlpea16040055

energy management and power-balancing strategies [11]. These approaches typically employ solar irradiance models for estimating the energy harvested from vehicle-mounted PV modules and use standardized driving cycles, such as the New European Driving Cycle (NEDC), the Worldwide Harmonized Light Vehicles Test Procedure (WLTP), and the Environmental Protection Agency (EPA) cycle, to evaluate energy consumption and vehicle performance. Previous studies, such as that reported in Ref. [12], have demonstrated that optimizing the PV design integrated into EVs can increase the driving range by up to 20%, even under variable shading conditions encountered during real-world operation.

Research on EV charging stations has addressed a wide range of technological challenges, including power electronics, energy management, system sizing, and techno-economic assessment. In the field of power electronics, several studies have investigated the implementation of Maximum Power Point Tracking (MPPT) algorithms integrated with power electronic converters (PECs) to optimize the charging process of different EV models and maximize the utilization of PV energy resources [13].

The feasibility of residential photovoltaic systems (RPVSs) for EV charging has also been evaluated through the analysis of energy generation and consumption under real operating conditions. For example, studies involving 4.48 kW PV installations have demonstrated the importance of aligning solar generation profiles with EV charging demand to improve energy utilization and reduce MG dependency [14].

Furthermore, techno-economic and environmental assessments have shown that the performance of charging infrastructures based on hybrid microgrids (μGs), integrating solar, wind, and diesel generation sources, strongly depends on the optimal sizing of both generation and ESS [15]. Parameters such as battery technology, charging duration, and projected demand have been identified as key factors influencing system reliability, operational stability, and economic viability [16].

The optimal sizing of standalone μGs has also been investigated using specialized simulation tools. For instance, the study presented in Ref. [17] proposes an 8.1 kW PV system integrated with an ESS capable of supporting the annual charging demand of up to 414 EVs with 30 kWh battery capacity. Beyond component sizing, the implementation of advanced Energy Management Systems (EMSs) has been recognized as a critical requirement for efficient system operation. As reported in Ref. [18], an effective EMS can reduce dependence on the MG by prioritizing PV generation and coordinating the use of EV batteries as distributed energy resources. Such strategies enable multiple operating modes, including renewable-only charging, MG-assisted charging, energy export to the MG, and battery discharging.

Similarly, studies focused on direct-current (DC) μGs for fast EV charging have highlighted the importance of considering charging demand patterns, baseline infrastructure consumption, and PEC efficiency when performing energy balance analyses and evaluating overall system performance [19].

The potential of EVs as distributed energy assets has also been analyzed at a national scale. For example, the study presented in Ref. [20] highlights that EVs remain parked for approximately 95% of their lifetime, representing a significant source of flexibility that can support power system operation and facilitate the large-scale integration of renewable energy sources, particularly solar generation.

To maximize this potential, smart charging strategies based on Grid-to-Vehicle (G2V), V2G, and V2V concepts have been proposed. These approaches commonly employ constant-current (CC) and constant-voltage (CV) charging techniques to improve charging efficiency and MG interaction. For instance, Ref. [21] analyzes a charging infrastructure composed of 200 charging stations rated at 22 kW and supplied by a 500 kW PV generation system.

In parallel, the development of scaled experimental prototypes has enabled the validation of standalone charging systems powered exclusively by PV generation and battery banks (BBs) [22]. These studies focus on the design and implementation of PECs capable of operating under variable solar irradiance conditions while maintaining stable output power and ensuring charging reliability.

Furthermore, comparative analyses have evaluated different EV charging architectures, including conventional MG-fed charging, extended-range EVs equipped with integrated PV modules, and solar-powered charging stations. These investigations have demonstrated that the integration of PV energy can reduce MG dependency and associated carbon emissions while improving the sustainability of electric mobility systems.

In Ref. [23], simulation-based analyses conducted for the cities of Berlin and Los Angeles demonstrated that although EVs equipped with integrated PV modules can extend driving range, solar-powered charging stations achieve superior performance in terms of energy efficiency and GHG emission reduction. Nevertheless, the reliance on purely numerical simulations underscores the need for experimental and real-time validation approaches capable of capturing the dynamic interactions among hardware components and energy management strategies.

Hardware-in-the-Loop (HIL) techniques have emerged as an effective alternative for the development and validation of EV-related technologies. For example, Ref. [24] presents the implementation of an EMS for the operation of an EV DC bus, integrating fuel cells and a BB to ensure power balance under varying generation conditions. Similarly, the development of model-free controllers for EV charging is evaluated in Ref. [25], demonstrating their capability to manage charging demand from multiple EVs.

Furthermore, the impact of EV integration on electrical distribution systems has been extensively investigated. The study reported in Ref. [26] analyzes key power quality indicators, including voltage profiles, power losses, and power factor variations at different points of the distribution network. Likewise, Ref. [27] highlights the importance of assessing distribution losses and harmonic distortion associated with V2G operation, emphasizing their influence on MG performance and reliability.

This paper presents an analysis of the dynamic interaction between a residential μG and an EV using a validation platform based on the HIL technique. The proposed μG is designed to maximize the utilization of PV energy while satisfying residential demand and considering the EV as an adaptive load. Both systems were modeled based on their power-flow dynamics and implemented on NI myRIO-1900 embedded controllers using the LabVIEW programming environment.

The developed HIL platform offers a high degree of reconfigurability, enabling the modification of key parameters such as the number of PV modules, ESS capacity, solar irradiance profiles, and MG interconnection voltage levels (120/240 V). Regarding the EV subsystem, the analysis focuses on battery energy behavior. An equivalent circuit model based on 18,650 lithium-ion cells, representative of the Tesla Model S BB, was implemented using parameters validated in literature [13].

The experimental evaluation is conducted under three operating scenarios: (1) EV charging supplied exclusively by the MG, (2) EV charging supplied by an isolated μG, and (3) EV charging supplied by a MG-connected μG. In Table 1 present a comparison with similar systems applied to EV charging process.

Table 1. Similar HIL platforms.

Reference	Contributions	HIL Platform	Reconfigurability	Process of Validation	Focus on
[9]	Uses continuous irradiance values to estimate SFR production	dSPACE MicroLabBox	At model level	Simulation	Design and control of PECs under simulated driving
[10]	The MATLAB Simulink software was used to evaluate the performance of MPPT algorithms, employing constant irradiance values while modifying the properties of the PEC used.	-	Allows for modification of the PV arrangement using the CEP elements and the values of the BB employed.	Simulation and comparation with databases	MPPT Control algorithm
[11]	They use PVWatts and representative irradiance estimates for different locations to estimate energy production.	-	It allows for an estimation of the energy that would be produced along a specific route.	Simulation	Transport and energy infrastructure planning
[14]	Presents the sizing for an off-grid (MG) load without interruptions, using data for a specific case of energy production and EV consumption.	PIC18F4550	No mentioned	Scale system and simulation	Controllers of PECs
[21]	Uses Modelica to compare the performance of an SFR under different climatic and irradiance conditions, as well as to compare different types of EVs.	-	Allows modification of the components used	Simulation	Comparison of energy demand versus production, considering different types of EVs
[24]	Use a rule-based EMS for the operation of PECs and fuel cells.	dSPACE MicroLabBox	No mentioned	Emulation in real time and theoretical data	Fuel cell vehicles and hybrid power systems
[25]	A J1772 protocol emulator is used for EV charging.	dSPACE MicroLabBox	EV with the same charging protocol	Emulation and real-world testing	Focused on reducing the effects on the distribution network
[27]	It uses confidential data in the experiments conducted and focuses on the MG model.	Global Real-Time Superlab (G-RTSLAB)	Modify the number and power level of the connected chargers	Emulation	Impact of the V2G and G2V paradigms on a Low Voltage MG
Our proposal	Interaction of μG (conformed by ESS, PV system and interconnection with MG) with BB of an EV to analyze energy exchange and EMS strategy based on utilization of PV generation to charge EV	NI MyRIO 1900	Define the components and properties of the μG elements, as well as the properties of the EV BB being used.	Emulation and model verification against published data	Energy exchange between uG and EV, allowing different EV BB configurations, PV systems and ESS, interaction is managed though EMS that could be modified or replace assuming correct design od different PECs used

The remainder of this paper is organized as follows. Section 2 describes the load emulation framework and the main system components, including the solar PV system, the μG, the MG, and the EV model. The operating conditions, charging protocols, and simulation parameters for the proposed scenarios are also presented. Section 3 details the mathematical models of the implemented systems and the procedures used to estimate

EV charging requirements and equivalent CO_2 emissions. Section 4 presents the experimental results obtained using the HIL platform. Section 5 provides a comparative analysis of energy consumption, operating costs, and environmental impact in terms of CO_2 emissions. Finally, Section 6 summarizes the main conclusions and contributions of this work.

The main contributions of this work are summarized as follows:

Development of a reconfigurable HIL platform: An HIL platform was designed and validated to emulate, in real time, the dynamic interaction between a residential μG and an EV. The proposed platform overcomes the limitations of purely numerical simulations by enabling the integration of realistic operating conditions and bidirectional energy flows between the system components.

High versatility for experimental analysis: The developed HIL platform allows real-time modification of critical variables, including solar irradiance profiles, ESS capacity, charging demand, and load profiles. This flexibility facilitates the evaluation of different operating scenarios and control strategies while avoiding the risks and costs associated with full-scale physical implementations.

Adaptability for energy management and charging strategies: The platform supports the implementation and validation of various EMS algorithms and EV charging methodologies. This capability enables the assessment of different control approaches according to the operational requirements of the μG and the charging demand of users.

Experimental validation of residential EV charging scenarios: The proposed system was experimentally evaluated under three operating conditions: MG-only charging, standalone PV charging, and MG-connected PV charging. This validation provides a comprehensive assessment of the technical and environmental performance of RPVS for EV charging.

Assessment of system scalability: Experimental tests were conducted using a RPVS originally sized for Level 1 EV charging. The system performance and operational stability were evaluated when higher charging-power demands were introduced, enabling the analysis of scalability and the feasibility of residential charging solutions under increased energy requirements.

The proposed system focuses on studying energy exchange between μG and EV, without considering other loads through the evaluation of an balance of energy equation; the developed HIL platform allows implementing domestic loads, but we are focusing on the energetic behavior of the charging process.

2. Description of the System

The main objective of this study is to evaluate the energy consumption, operating costs, and associated CO_2 emissions of EV charging under three different electrical supply architectures. To achieve this objective, a RPVS is integrated as a RES into the proposed charging schemes. Two PV operating configurations are considered: an isolated (off-MG) system and an MG-connected system interfaced with the MG. Both configurations are designed to represent residential AC applications and to assess the technical and environmental performance of EV charging under realistic operating conditions.

2.1. Microred

The proposed AC μG operates at nominal voltage levels commonly available in the MG, namely 120 V and 240 V. The DER consists of an RPVS configured using monocrystalline PV modules rated at 350 W. These modules were selected due to their high conversion efficiency. The ESS is composed of lithium-ion batteries with configurable charging and discharging profiles. PECs are employed to interconnect the different components of the μG, with their topology selected according to the characteristics of each component

and the required power flow. Figure 1 illustrates the architecture of the proposed μG and the interaction among its principal elements.

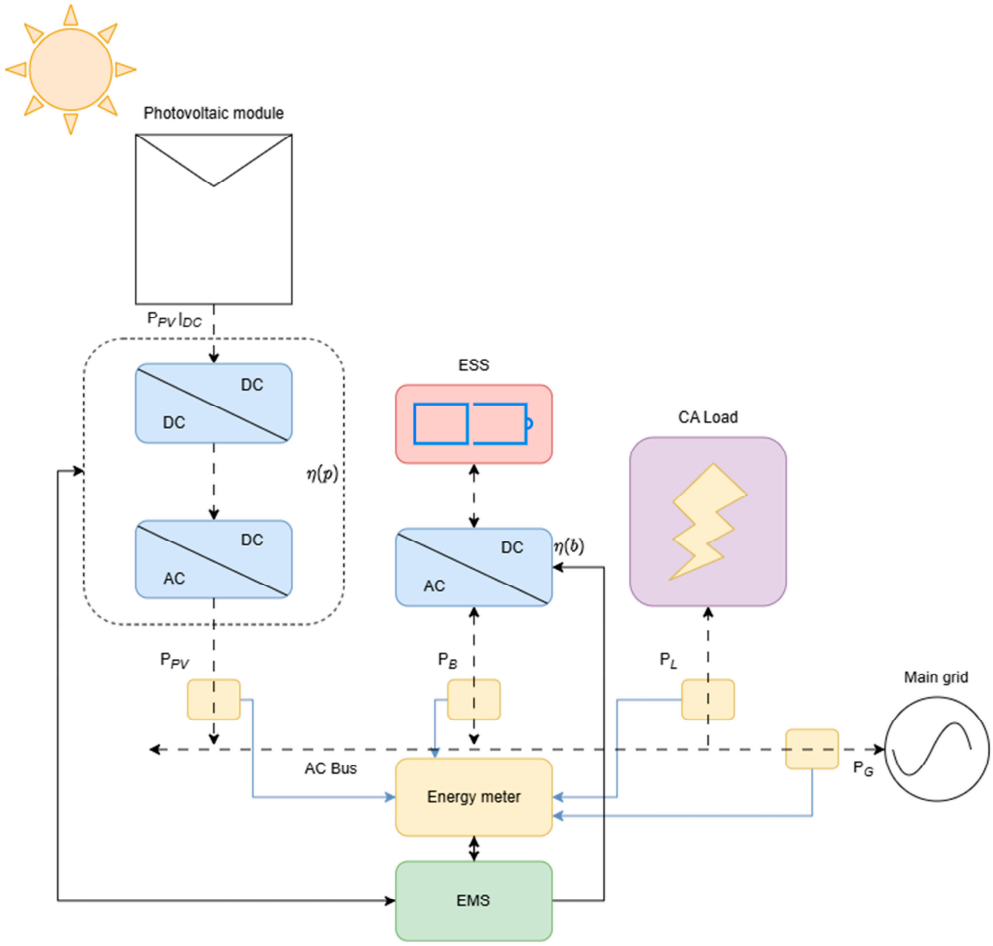


Figure 1. Architecture of the proposed microgrid.

The EMS supervises the operation of the μG and determines its operating mode. Depending on the conditions defined by the user, the EMS allows the μG to operate either in MG-connected mode or as an islanded system. The EMS is also responsible for coordinating power exchanges among the RPVS, ESS, loads, and the MG in order to maintain energy balance and ensure system stability.

Within the proposed μG, a sign convention is adopted for power flow analysis. Positive power values indicate that a component is supplying energy to the AC bus, whereas negative values indicate that the component is consuming energy from the AC bus. Consequently, the PV power (P_{PV}) is always positive because the RPVS only injects energy into the system. Conversely, the load power (P_L) is always negative since residential loads and EV chargers consume energy from the AC bus.

The power associated with the MG P_G and the ESS P_B may be either positive or negative depending on the operating mode. The value of P_G is positive when energy is imported from the MG to supply the AC bus and negative when excess energy generated by the RPVS is exported to the MG. Similarly, P_B is positive when the BB discharge energy to the AC bus and negative when the ESS is being charged. An energy monitoring module is incorporated into the μG to quantify power exchanges among components and evaluate the environmental impact of the different operating scenarios.

For modeling purposes, the losses associated with MG are neglected. The RPVS employs a DC-DC PEC operating under a MPPT algorithm to maximize PV energy extraction. In addition, a proportional-integral (PI) controller regulates the operating voltage of

the PV subsystem. A DC-AC PEC is used to transfer energy from the RPVS to the AC bus. The ESS is interfaced through a bidirectional AC-DC PEC (rectifier/inverter), which enables both battery charging and discharging while facilitating bidirectional energy exchange between the BB and the AC bus.

Energy Management System

The primary objective of the EMS is to maintain the stability of the AC bus while maximizing the utilization of the energy generated by the RPVS. Figure 2 presents the EMS control algorithm, which is based on the following operating strategies:

Maintaining AC bus voltage stability.

Maximizing the utilization of RESs.

Keeping the battery State of Charge (SoC) within safe operating limits.

Minimizing the operating cost associated with energy consumption.

To accomplish these objectives, the centralized EMS [28] determines the operating mode of each subsystem within the μG by coordinating the local controllers associated with the PECs. The decision-making process is based on the EV charging demand and the energy availability from the RPVS, the ESS, and the MG.

The EMS establishes an energy dispatch hierarchy in which PV generation is prioritized as the primary energy source due to its renewable nature and negligible operating cost. When the available PV power is insufficient to satisfy the demand, the required energy is supplied by the MG. The ESS is used as a complementary energy source to support system operation and maintain power balance. Since the stored energy involves additional costs associated with battery charging, storage, and degradation, its utilization is prioritized after the RPVS and the MG.

Based on the operating principles described above, the EMS defines the following operating cases:

Case 1. PV generation matches the load demand.

When the available PV power P_{PV} is equal to the total load demand P_L, the RPVS operates as the sole energy source supplying the AC bus.

Case 2. PV generation is insufficient to satisfy the load demand

When $P_{PV} < P_L$, the power deficit must be supplied either by the MG or by the ESS.

(a) If the MG is available, the required additional power is imported from the MG to satisfy the load demand $P_G = P_L - P_{PV}$.

(b) If the MG is unavailable, the energy supply depends on the battery SoC:

(i) If the SoC is greater than 30%, the ESS supplies the remaining power required by the load $P_B = P_L - P_{PV}$.

(ii) If the SoC is less than or equal to 30%, the ESS is disconnected to prevent excessive battery discharge. Under this condition, the load demand cannot be satisfied, and the system operation is interrupted $P_G = P_B = P_{PV} = 0$.

Case 3. Excess PV generation

When $P_{PV} > P_L$, excess energy is available and must be directed either to the ESS or to the MG.

(a) If the ESS SoC is below 80%, the excess PV energy is used to charge the ESS $P_B = P_{PV} - P_L$.

(b) If the ESS SoC is greater than or equal to 80% and the MG is available, the excess energy is exported to the MG $P_G = P_{PV} - P_L$.

(c) If the ESS SoC is greater than or equal to 80% and the MG is unavailable, the PV controller limits the generated power by switching from MPPT mode to voltage-control mode, thereby regulating the energy delivered to the load and maintaining system stability $P_{PV} = P_L$.

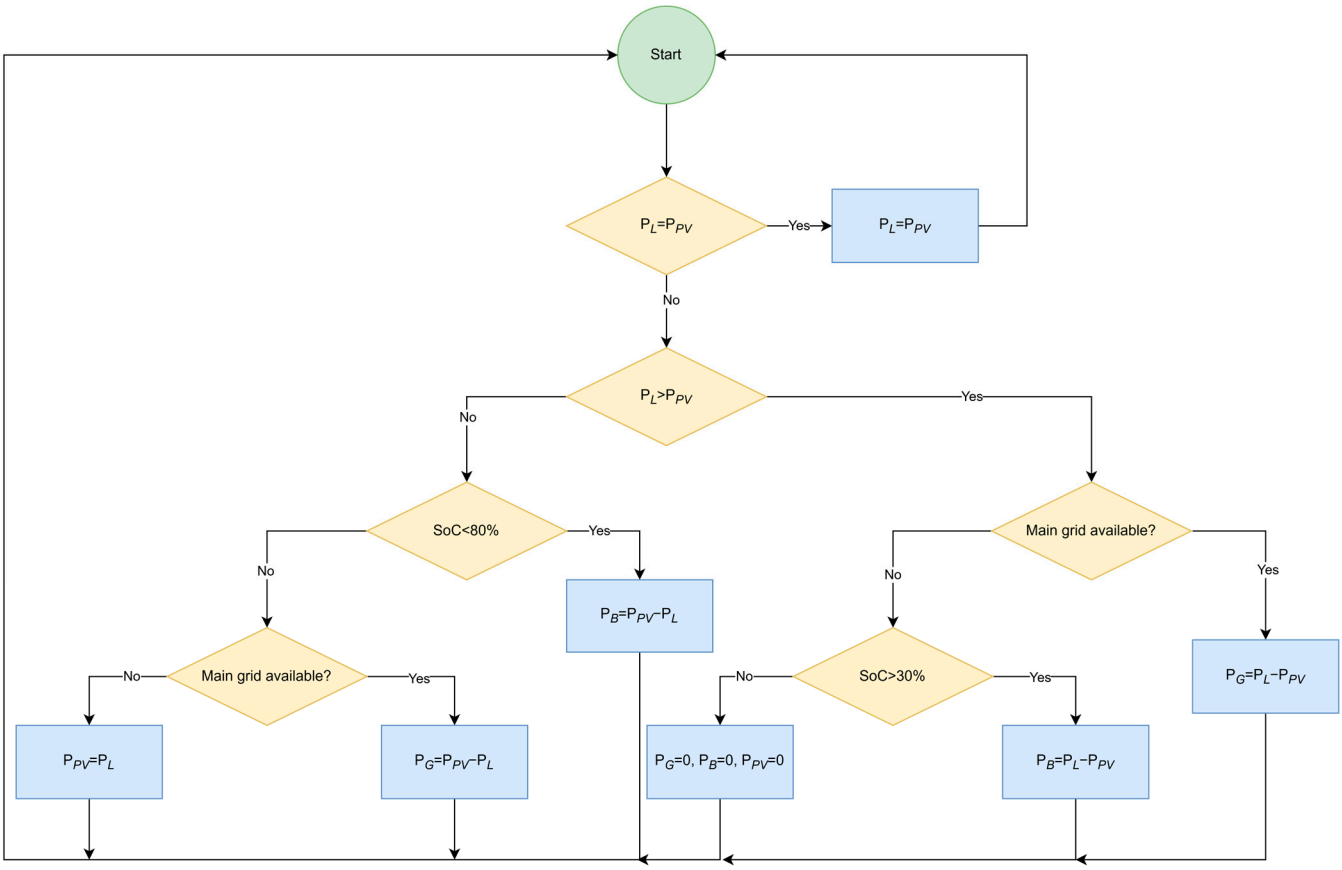


Figure 2. Flowchart of the proposed Energy Management System.

2.2. Electric Vehicle

The EV considered in this study is composed of a BB as ESS, PECs, and electric traction motors operating under either AC or DC architectures. Currently, EV battery technologies are not fully standardized, resulting in significant variations in battery chemistry, capacity, and operating characteristics [7,29]. Among the available technologies, lithium-ion batteries have become the preferred choice due to their high energy density, long cycle life, and superior charge/discharge performance. In this work, the analysis focuses exclusively on the EV charging process. Therefore, only the EV battery system and its charging interface are considered, while the traction system and vehicle dynamics are excluded from the study. The experimental platform is based on the battery characteristics of the Tesla Model S, which employs battery packs composed of 18,650 lithium-ion cells. Since the objective is to evaluate the energy exchange between the μG and the EV during charging, it is necessary to model the electrical behavior of both the battery pack and the charging system. Accordingly, the charger operating characteristics and charging demand profile were implemented according to the specifications reported in the literature [11,18,30,31].

Electric Vehicle Charging Standards

The charging process of EV batteries can vary considerably depending on the charger technology, power level, and electrical architecture employed. International organizations, such as the Society of Automotive Engineers (SAE) and the International Electrotechnical Commission (IEC), have established standards to classify EV charging systems according to the voltage, current, and charging method used in both AC and DC applications. The SAE standard classifies charging infrastructure into different charging levels according to the supplied power and charging requirements, whereas the IEC standard

defines charging modes based on the electrical connection and safety features implemented during the charging process. A summary of the most common charging standards and their characteristics is presented in Table 2 [23].

Table 2. Electric vehicle charging standards.

Standard	Voltage (V)	Current (A)	Mode/Level	Fase
IEC62196	120	16	Mode 1	AC
	240	32	Mode 2	
	250	32–250	Mode 3	DC
	600	400	Mode 4	
IEC62196	120	16	Mode 1	AC
	240	80	Mode 2	
	240–450	80	Mode 4	DC
SAEJ1772	120	16	Level 1	AC
	240	32–80	Level 2	
	200–450	80	Level 1	DC
		200	Level 2	

According to these standards, portable chargers operating at 120 V AC are generally classified as Level 1 chargers under the SAE J1772 [32]standard and as Mode 1 chargers under the IEC 62196 [33]framework. Chargers connected to dedicated 240 V residential circuits are commonly classified as Level 2 or Mode 2 charging systems, depending on the standard being applied [34]. Furthermore, dedicated charging stations support higher-power charging configurations, including AC charging modes and DC fast-charging technologies associated with IEC Modes 3 and 4. The EV considered in this investigation, a Tesla Model S, can be charged using either a portable charging cable or a wall-mounted charging connector. When a portable charger is used, the EV can be connected to either 120 V or 240 V AC supplies, enabling Level 1 or Level 2 charging operation depending on the available voltage. In contrast, wall-mounted charging equipment typically requires a dedicated 240 V AC installation, allowing higher charging power and reduced charging times. Several charging methods have been proposed for lithium-ion batteries, including CC charging, CV charging, the combined Constant Current–Constant Voltage (CC-CV) method, and pulse-charging techniques [35]. In the present study, the charging process is implemented using the CC method, since this approach is consistent with the charging characteristics reported for the Tesla Model S battery pack and facilitates the evaluation of energy consumption under controlled operating conditions.

2.3. Proposed Emulation System

The developed HIL platform was implemented using two NI myRIO-1900 embedded controllers Manufactured by National Instruments (NI), based in Austin, Texas, United States. One controller executes the residential μG model, while the second controller emulates the EV. The proposed charging emulation system is illustrated in Figure 3. Each myRIO-1900 controller executes an independent Virtual Instrument (VI) developed in the LabVIEW environment, enabling the real-time emulation of both the μG and EV subsystems. The two VIs communicate with a supervisory VI executed on a host computer, which provides the graphical user interface (GUI) for user interaction. Through this interface, the user can configure the operating conditions and define the electrical and operational parameters of both the μG and the EV. In addition, the two myRIO controllers exchange information through analog signals that represent the electrical variables required for the EV charging process, enabling real-time interaction between the emulated systems. The developed LabVIEW interface allows the user to modify the number of PV modules

integrated into the RPVS, each with a nominal generation capacity of 350 W. The PV generation depends on the solar irradiance (G_T) applied to the PV modules. Irradiance profiles are introduced as time-series vectors and can be imported directly from Microsoft Excel files. For the ESS, the user can define the number of batteries connected in series and specify the initial SoC. The operating condition of the MG interconnection and the nominal voltage of the AC bus are also configured through the user interface. A MG voltage of 0 V represents a MG outage or disconnection event, whereas voltage levels of 120 V and 240 V correspond to the standard residential AC operating conditions considered in this study.

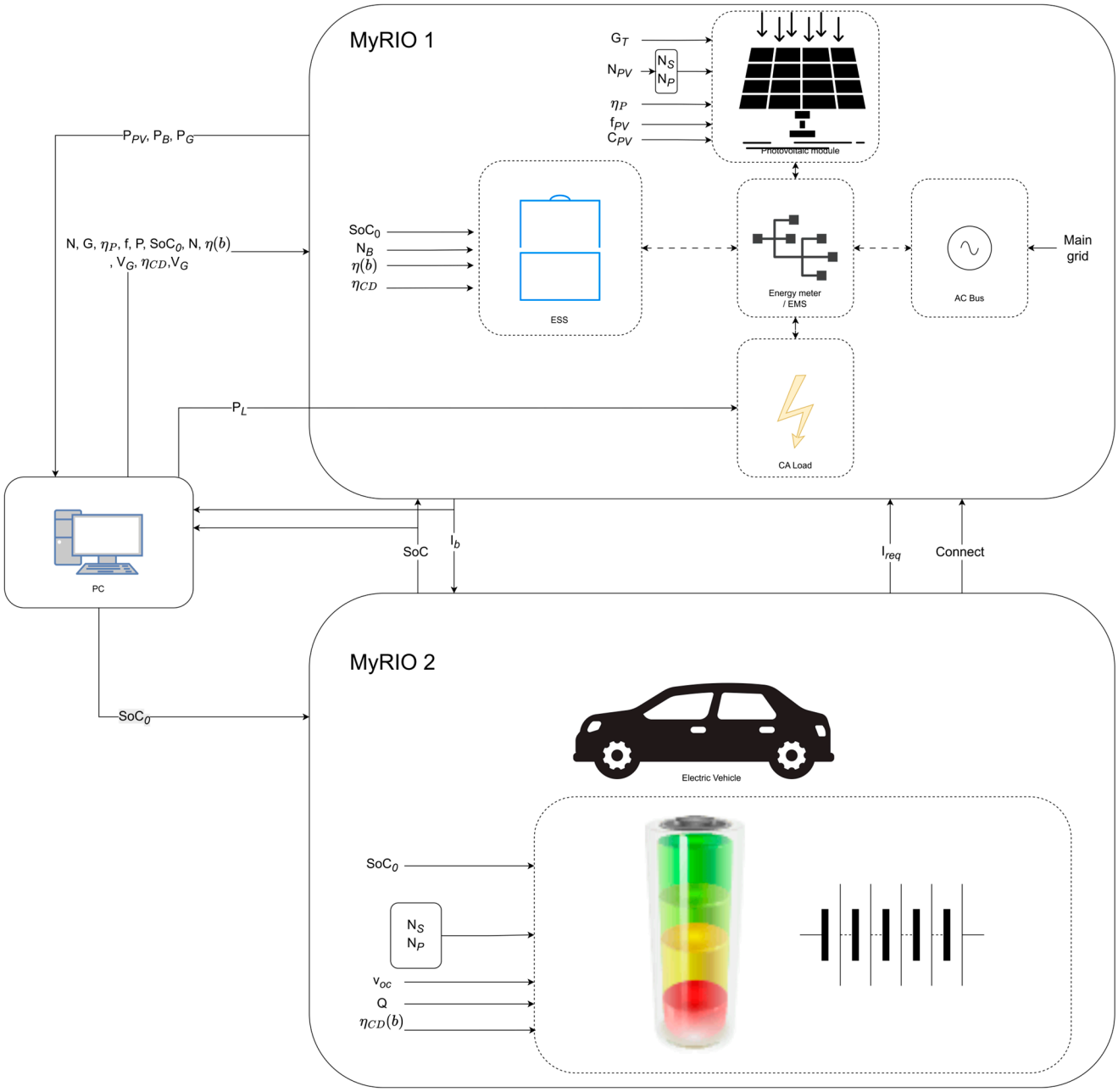


Figure 3. Proposed electric vehicle charging emulation system.

Most of the parameters associated with the proposed Charging Emulation System (CES) are configured through the VI executed on the host computer. However, certain parameters must be defined locally within the VIs implemented on each embedded system. In the case of the EV model, it is necessary to specify the number of battery cells connected in series and parallel in order to define the battery pack configuration. The CES

requires G_T and load demand profiles P_L as input variables. The irradiance data employed in this study correspond to a typical sunny summer day in the city of Celaya, Mexico. These irradiance profiles were estimated from the energy production data of an installed RPVS with known nominal power, allowing the reconstruction of the corresponding solar resource profile. The load demand profile P_L can be defined in two different ways:

Residential load profile: The demand is established using previously recorded residential consumption data.

EV charging load profile: The demand is determined by the connection and charging process of the EV, according to the selected charging conditions and battery parameters.

Due to the purpose of this work being analyzing the energetic behavior of EV charging using RPVS, residential load profiles are excluded because considering a residential load involves energy consumption separate from that generated by the EV charging process, which is the subject of this study.

To validate the operation of the proposed CES, three different charging scenarios were evaluated.

Scenario 1. EV charging supplied exclusively by the MG. In this scenario, the EV is charged using only the energy supplied by the MG, separate in two cases (Level 1 and Level 2): Scenario 1 Level 1 operating at a nominal voltage of 120 V AC and Scenario 1 Level 2 operating at nominal voltage of 240 V AC. The RPVS generation is set to zero, while the ESS remains inactive due to the availability of MG power. The EV charging process is performed according to Level: Level 1 charging requirements, allowing a maximum charging power of up to 1.9 kW and Level 2 charging requirements, allowing a maximum charging power of up to 11 kW.

Scenario 2. EV charging supplied by an isolated μG. In this case, the μG operates in stand-alone mode without connection to the MG. The ESS is initialized with an SoC of 80%, while the RPVS is configured with a maximum generation capacity of 10 kW. The EV charging process is performed under Level 2 charging conditions, allowing a maximum charging power of up to 11 kW.

Scenario 3. EV charging supplied by an MG-connected μG. In this scenario, the μG operates interconnected with the MG, which is configured at 240 V AC. The ESS is initialized with a SoC of 80%, and the RPVS is configured with a maximum generation capacity of 10 kW. Similar to Scenario 2, the EV charging process follows Level 2 charging requirements, with a maximum charging power of up to 11 kW.

For all three scenarios, the residential load is assumed to be zero. Therefore, the μG is dedicated exclusively to supplying the power required for the EV charging process, allowing the analysis to focus on the interaction between the EV, the RPVS, the ESS, and the MG.

This methodology was selected because we do not have the infrastructure to compare results against real values with EV chargers and PV systems. The HIL technique allows us to realize experiments using mathematic models executed in hardware under controlled conditions.

To design platform models and assumptions of related works where used, the verification process considers data available in databases and published works. Particularly for EV, results of emulations are compared with published works.

The developed platform can be accessed via [36]; the repository contains the requirements data and instructions.

3. Modeling of the Charging Emulation System

To implement the different subsystems within the proposed CES, it is necessary to develop their corresponding mathematical models and subsequently discretize them for

real-time execution in the HIL platform. The resulting models enable the emulation of the dynamic interactions among the μG, the EV, and the EMS. For modeling purposes, the PECs included in the CES are represented through their conversion efficiencies. Therefore, it is assumed that the converters and their associated local control systems are properly designed and operate within their nominal conditions, such that their dynamic effects do not significantly influence the overall performance of the proposed system. This simplification allows the analysis to focus on the energy exchange among the principal components of the μG and the EV charging process.

3.1. Microgrid Modeling

The proposed μG consists of an RPVS, an ESS, an interconnection with the MG, electrical loads, and an EMS. The interaction among these components enables the coordination of energy generation, storage, and consumption while maintaining the power balance of the μG. The EMS supervises the operation of the μG and manages the power exchange between the RPVS, ESS, MG, and connected loads. Depending on the operating conditions, the μG can operate either in MG-connected mode or in islanded mode, ensuring the continuity of supply and maximizing the utilization of RERs.

3.1.1. Residential Photovoltaic System

The power generated by a RPVS can be estimated using different modeling approaches. One of the most widely used methods is based on simulation tools such as PVWatts, which require the definition of environmental conditions, PV module characteristics, and PEC efficiencies. Alternatively, the output power of a RPVS can be estimated using mathematical models that relate the incident solar irradiance to the electrical power generated by the PV array. In this work, the power produced by the RPVS is determined using a simplified irradiance-based model, in which the generated power is proportional to the solar irradiance incident on the PV modules. This relationship can be expressed as follows [9,13,17,18]:

$$P_{PV}|_{DC} = C_{PV} f_{PV} \left(\frac{G_T}{G_{T,STC}} \right) \times [1 + \propto_P (T_C - T_{C,STC})] \quad (1)$$

where

C_{PV}: nominal power of the RPVS (W).
G_T: solar irradiance incident on the PV array (W/m²).
$G_{T,STC}$: solar irradiance under STC, equal to 1000 W/m².
$\propto_P$: temperature coefficient of power (%/°C).
T_C: PV cell temperature (°C).
$T_{C,STC}$: PV cell temperature under STC, equal to 25 °C.
f_{PV}: aging factor.

Equation (1) allows the estimation of the electrical power generated by a photovoltaic (PV) module. Therefore, when multiple PV modules are connected in series, parallel, or series-parallel configurations, the total generated power depends on the number of modules installed and their electrical arrangement. In this study, thermal losses and efficiency degradation effects are neglected. Furthermore, it is assumed that the solar irradiance is uniformly distributed across all PV modules. Under these assumptions, the mathematical model adopted for the RPVS is represented by Equation (2).

$$P_{PV} = \eta_P N_{PV} C_{PV} f_{PV} \left(\frac{G_T}{G_{T,STC}} \right) \quad (2)$$

For the operation of the RPVS, either in Voltage Control Mode (VCM) or MPPT mode, it is necessary to consider the PECs and their corresponding efficiencies. One PEC is

responsible for extracting the maximum available power from the PV array, while another PEC transfers the generated energy to the AC bus. The RPVS is assumed to operate in MPPT mode under normal conditions in order to maximize energy harvesting from the PV modules [10,37]. However, when the generated PV power exceeds the load demand and no additional energy sink is available, the controller switches to VCM to regulate the power delivered by the RPVS and maintain system stability. To establish the PEC efficiency values used in this investigation, the data reported in [38] were adopted. According to this reference, the DC-DC PEC efficiency is assumed to be 0.80, while the DC-AC inverter efficiency is assumed to be 0.85. These values are used to determine the overall efficiency of the PV generation subsystem $\eta_P = 0.8 \times 0.85 = 0.68$.

3.1.2. Energy Storage System

The ESS is composed of lithium-ion batteries due to their advantages over other battery technologies, including high energy density, long cycle life, and superior charge–discharge performance [7,39]. To model the ESS, it is necessary to estimate the battery State of Charge (SoC), which represents the amount of energy stored relative to the battery's nominal capacity. Several methods for SoC estimation have been reported in the literature [40–42].

To estimate the SoC, the coulomb-counting method was adopted, as expressed in Equation (3). The SoC is calculated from an initial state of charge (SoC_0), considering the battery charge/discharge efficiency η_{CD} and the nominal battery capacity Q (Ah). In addition, it is necessary to determine the battery current i_b, which is obtained from the charging or discharging power exchanged by the battery [43]. The open-circuit voltage of the battery, Voc, is subsequently determined using Equation (4). To construct the ESS employed in this study, four battery modules were considered as the base configuration. Each module is composed of series-connected cells and provides a nominal voltage of 12 V, a rated capacity of 115 Ah, and a charge/discharge efficiency of 0.9 [40]. The total number of battery modules incorporated into the ESS is represented by NB:

$$\mathrm{SoC} = SoC_0 + \frac{\eta_{CD}}{Q}\int_{t_0}^{t} i_b\, dt \tag{3}$$

$$Voc = 3.3 + 0.6 \times (\mathrm{SoC} - 0.08 \times \mathrm{SoC} \times (1 - \mathrm{SoC}))) \tag{4}$$

For the charging and discharging operation of the ESS, two bidirectional PECs are considered. The first PEC operates as a rectifier/inverter, enabling the conversion between AC and DC power, while the second PEC functions as a bidirectional DC-DC PEC responsible for regulating the charging and discharging processes of the ESS. For the experiments presented in this work, an efficiency of 0.96 is assumed for each PEC. Since the PECs are connected in cascade, the overall conversion efficiency is determined by the product of the individual PEC efficiencies obtaining $\eta(b) = 0.9216$. The ESS, P_B, is calculated from the μG power balance. Based on the SoC of the ESS, the stored energy can be determined and subsequently used to estimate the battery current. This current is then employed to calculate the variation of the SoC according to Equation (5) where a value f is used. The value of P_B depends on the direction of the power flow. During the charging process, P_B is negative because energy is absorbed by the ESS, and f takes the value of $\eta(b)$. Conversely, during the discharging process, P_B is positive because energy is supplied by the ESS to the AC bus; in this case, f takes the value of $\frac{1}{\eta(b)}$.

$$i_b = \frac{P_B}{Voc} \times f \tag{5}$$

3.1.3. Energy Management System

To coordinate the operation of the components that constitute the μG, a centralized EMS is implemented. The EMS operation is based on the power balance equation given in Equation (6), which represents the energy equilibrium of the system according to the sign convention described in Section 2. Based on this power balance, the EMS determines the operating state of each subsystem and selects the appropriate control actions for the RPVS, the ESS, and the MG. The corresponding operating modes and decision rules were previously described in Section Energy Management System.

$$P_G + P_L + P_{PV} + P_B = 0 \quad (6)$$

3.2. Electric Vehicle Modeling

The battery model used for the EV emulation in this study is based on 18,650 lithium-ion cells, a technology commonly employed in Tesla EV. Using the parameters reported in Ref. [44], the information available in Ref. [45], and the specifications provided by the manufacturer, the battery pack of a Tesla Model S Plaid was selected as the reference system. The battery pack operates at a nominal voltage of 407 V and a nominal capacity of 246 Ah, comprising a total of 7920 cells arranged in a configuration of 110 cells connected in series and 72 cells connected in parallel, resulting in a nominal energy capacity of approximately 100 kWh. Figure 4 presents the equivalent RC circuit used to model an individual battery cell. Similar to the ESS model described previously, the SoC of each cell is estimated using the coulomb-counting method. The corresponding mathematical formulation is given in Equation (7). The output voltage of the cell is determined from the voltage drops across the elements of the equivalent circuit model and is represented by Equations (8)–(10) [44]. In these equations, R_1 and C_1 represent the resistor and capacitor associated with the polarization branch RC_1 with voltage V_{RC_1}, R_2 and C_2 represent the resistor and capacitor associated with the polarization branch RC_2 with voltage V_{RC_2} respectively, Ro represents the internal resistance of the cell, Voc denotes the open-circuit voltage, and VL corresponds to the terminal voltage of the battery cell.

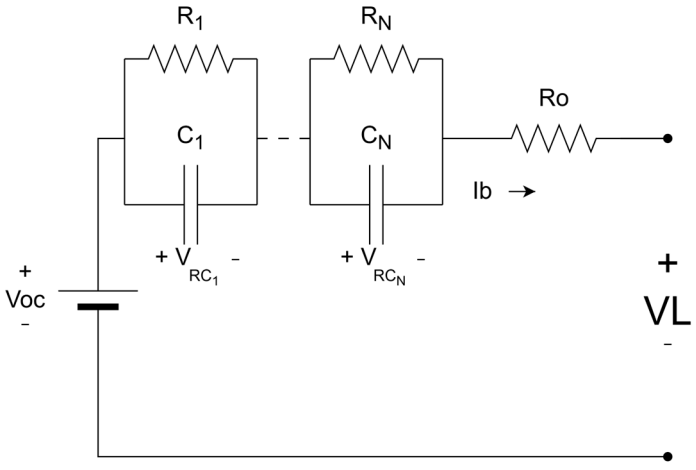


Figure 4. Equivalent RC circuit model of the EV battery cell.

$$V_{OC} = 12.2581 \times SoC^6 - 28.8126 \times SoC^5 + 20.7236 \times SoC^4 - 2.6045 \times SoC^3 - 1.9103 \times SoC^2 + 1.0889 \times SoC + 3.4444 \quad (7)$$

$$\dot{V_{RC_1}} = -\frac{V_{RC_1}}{R_1 C_1} + \frac{I_b}{C_1} \quad (8)$$

$$\dot{V_{RC_2}} = -\frac{V_{RC_2}}{R_2 C_2} + \frac{I_b}{C_2} \quad (9)$$

$$VL = V_{OC} - V_{RC_1} - V_{RC_2} - I_b \times Ro \quad (10)$$

The battery cell model described previously was used as the basis for constructing the battery pack of the Tesla Model S. For this purpose, it was necessary to define the number of cells connected in series and parallel, allowing the battery capacity and voltage configuration described in Section 3.2 to be obtained. The resulting battery-pack characteristics are determined according to Equations (11) and (12).

$$\mathrm{Q}_T = N_P \times Q \quad (11)$$

$$V_T = N_S \times V_{OC} \quad (12)$$

3.3. Energy Consumption, Cost, and Emissions Analysis

In Mexico, the Federal Electricity Commission (CFE) is the entity responsible for the supply and billing of electrical energy. The nominal voltage for residences is 120 V AC; if an SFR is present, a 240 V AC installation is required. For residential users, CFE applies different tariff schemes depending on the level of electricity consumption and the average minimum summer temperature corresponding to each geographical region. Residential electricity tariffs are classified as 1, 1A, 1B, 1C, 1D, 1E, and 1F. Electricity costs are calculated according to a block-rate structure composed of basic consumption ($1.11/kWh), intermediate consumption ($1.349/kWh), and excess consumption ($3.944/kWh). The consumption limits associated with each block depend on the assigned tariff category and the corresponding two-month billing period. When the average electricity consumption exceeds the limit established for the applicable tariff, the customer is reclassified under the High Consumption Domestic (DAC) tariff. Under this scheme, billing includes a base consumption equivalent to the first 25 kWh defined in Tariff 1, as well as a fixed monthly charge and a variable charge proportional to the energy consumed. Both charges depend on the tariff region assigned by CFE. In the case of Celaya, Guanajuato, which belongs to the South-Central tariff region, the fixed monthly charge is 142.41 MXN, while the cost of electricity consumption is 6.169 MXN/kWh. Consequently, exceeding the consumption limits established under conventional residential tariffs can significantly increase the total electricity cost [46].

When an SFR is in place, the billing rate remains the same as that of a standard residential system, that is, the rate structure does not change. In this scenario, the number of kWh consumed is based on the net consumption from MG; in other words, it is the difference between the energy imported from MG and the energy exported to MG in the corresponding period; if this value is less than zero, it is considered zero.

To quantify the environmental impact associated with EV charging, the equivalent CO_2 emissions are estimated using Equation (13) [47]. The emissions are calculated as a function of the electrical energy consumed and the national electricity generation emission factor F_E. For the year 2024, the Mexican national MG emission factor was considered as 0.444 tCO_2/MWh, equivalent to 0.444 $kgCO_2$/kWh. Therefore, the total CO_2 emissions associated with energy consumption can be determined as follows:

$$E_{CO_2} = E_P \times F_E \quad (13)$$

where

E_{CO_2}: equivalent carbon dioxide emissions ($kgCO_2$).

E_P: electrical energy consumption (kWh).

F_E: grid emission factor (kgCO_2/kWh).

3.4. Electric Vehicle Charging Calculation

The charging power of the EV depends on the selected charging mode and charging level. Since a CC charging strategy was adopted in this study, the electrical power delivered to the battery is determined as a function of its nominal capacity $Q \times \%C$ and must be consistent with the rated output power of the charger. Accordingly, if the required charging current is represented by I_{Req}, the charging power and the current drawn from the AC bus I_{Ext} can be calculated using Equations (14) and (15), respectively. The charging process is constrained by both the charger specifications and the operating limits of the EV battery pack, ensuring safe operation and compliance with the selected charging standard.

$$I_{Req} = Q \times \%C \tag{14}$$

$$I_{Ext} = I_{Req}/\eta_{CD}(b) \tag{15}$$

The power import from the MG depends on the operating voltage of the MG. For these calculations, it is assumed that the EV battery voltage remains constant at its nominal value throughout the charging process. In Scenario 1, the EV charging process is carried out under Level 1 and Level 2 charging conditions, requiring a charging power of 1.9 kW and 11 kW. Based on this charging power and the nominal battery voltage, the corresponding charging current $I_{Req} = 1900/407 = 4.66$ A and the charging rate $\%C = 4.66/246 = 0.018$ are obtained, resulting in a charging rate of approximately 0.018 C for Level 1. For Scenarios with Level 2, the EV charging process is performed under Level 2 charging conditions with a maximum charging power of 11 kW, resulting in a charging rate of approximately 0.1098 C.

The proposed μG must supply the power required by the EV charging process. This value is calculated from the power delivered to the EV battery P_L and the efficiencies of the PECs involved in the charging process. In this work, the charger efficiency $\eta_{CD}(b)$ is assumed to be 0.92. Knowing the energy delivered to the battery and the battery terminal voltage VL, the EV charging power P_{EV} can be determined. Consequently, the power demand imposed by the EV charging system is calculated according to Equation (16).

$$P_L = P_{EV}/\eta_{CD}(b) \tag{16}$$

4. Results

4.1. Validation of the Charging Emulation System

To validate the performance of the developed HIL platform, two validation experiments were conducted. The first experiment was based on the charging characteristics of a Tesla Model S reported in Ref. [10], while the second employed the charging data of a Škoda CITIGOe iV EV reported in Ref. [12]. For both validation cases, ideal operating conditions were assumed, considering the same efficiency for both the PECs and the EV charger as in the rest of the paper. Table 3 indicates the models used and where values of efficiency used in this work were found.

Table 3. Summary of models and considerations in the development of this HIL platform.

Component	Modeled As	Taked From
RPVS	Equation of generated power based on measured irradiance	[9,13,17,18]
BB used as ESS in μG	Power exchange and coulomb counting method	[40–42]
PECs	Efficiencies	[38,40]

EV BB	Equivalent circuit model of two RC branches	[43]
EV Charger PECs	Efficiencies	Datasheet of chargers

In the first validation experiment, the charging process of the Tesla Model S battery was simulated using a CC charging strategy. The battery SoC was increased from 0% to 100% using an average charging power of 10.8 kW supplied by a Level 2 charging station. Figure 5 shows the evolution of the battery SoC, represented by the red curve. The developed HIL platform predicts a charging time of 11.2 h to increase the SoC from 0% to 100%, whereas the charging time reported in Ref. [10] is 10.5 h. Therefore, the relative error between the simulated and reported results is 6.7%, indicating good agreement between the proposed emulation platform and the reference data. The obtained results demonstrate that the developed HIL platform accurately reproduces the charging behavior of the Tesla Model S battery and is suitable for evaluating EV charging scenarios under different microgrid operating conditions.

Figure 5 also presents the power exchange among the components of the proposed μG during the EV charging process. The yellow curve represents the power generated by the RPVS, the blue curve corresponds to the power imported by the MG, the purple curve indicates the power exported to MG, and the black curve represents the charging power delivered to the EV battery. Once the EV is connected, two operating conditions are observed:

Case 1: During periods of high PV generation, the power produced by the RPVS exceeds the EV charging demand. Consequently, the excess energy is exported to the MG.

Case 2: When the EV charging demand exceeds the power generated by the RPVS, the deficit is supplied by the MG, thereby ensuring uninterrupted charging operation.

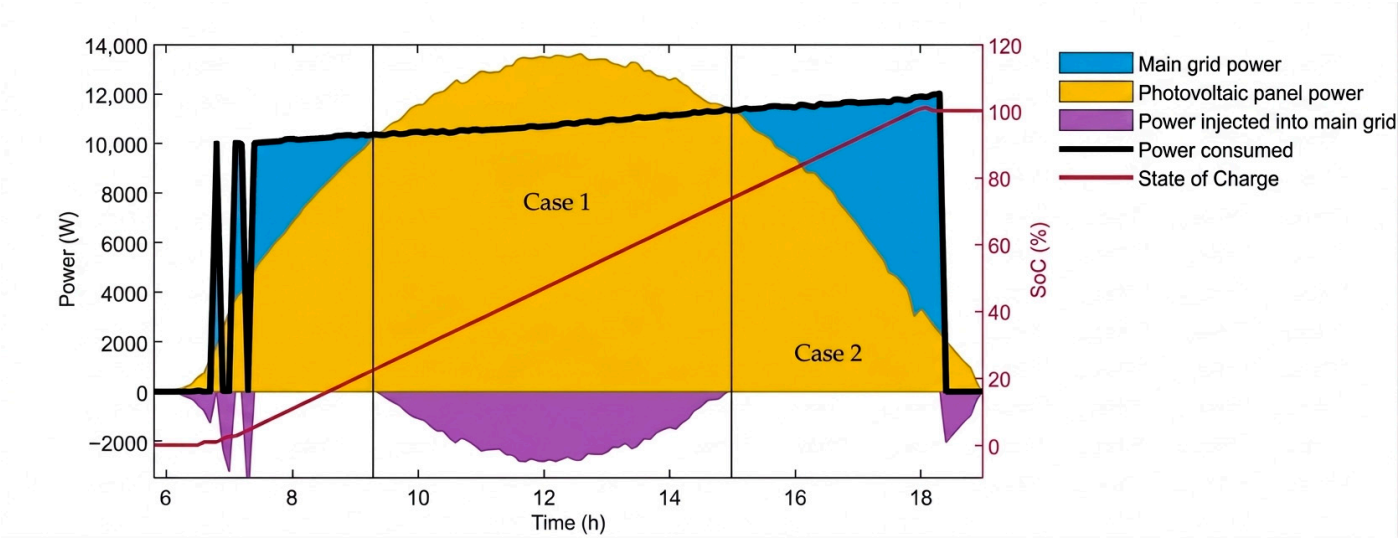


Figure 5. Charging emulation results for the Tesla Model S.

During the second validation experiment, the charging process reported in Ref. [12] was reproduced using the proposed HIL platform. The referenced study employed a residential charger specifically designed for the Škoda CITIGOe iV, increasing the battery SoC from 15.2% to 95.6% for a battery pack with a nominal capacity of 36.8 kWh over a charging period of 16 h using a CC charging strategy. During the charging process, the battery voltage varied from 296.25 V to 351.75 V. Since the battery cell specifications were not provided in Ref. [12], a battery configuration was designed to closely match the reported voltage and energy capacity. The resulting battery pack consists of 86 cells connected in series and 33 branches connected in parallel, yielding a nominal voltage of 326.8 V, a capacity of 112.2 Ah, and a total energy capacity of 36.67 kWh. These values closely

approximate those reported for the Škoda CITIGOe iV battery pack. Figure 6 presents the evolution of the battery SoC during the emulation process, represented by the red curve. The developed model successfully reproduced the charging behavior reported in Ref. [12], achieving a relative error of only 0.625% with respect to the reported battery energy capacity of 36.8 kWh. This result confirms the accuracy of the proposed HIL platform for EV charging emulation.

Figure 6 also illustrates the power exchange among the components of the proposed μG during the charging process. The purple curve represents the power exported to the MG, the blue curve corresponds to the power imported from the MG, the yellow curve indicates the power generated by the RPVS, the red curve represents the power supplied by the ESS, and the black curve denotes the charging power delivered to the EV battery. At the beginning of the experiment, the EV is disconnected from the μG. Once PV generation becomes available, the generated energy is initially directed toward charging the ESS because the battery SoC is below 80%. When the EV is connected to the μG, four operating conditions can be identified:

Case 1. The power generated by the RPVS exceeds the EV charging demand. Therefore, the excess energy is used to charge the ESS.

Case 2. The power generated by the RPVS exceeds the EV charging demand and the ESS reaches an SoC of 80%. Consequently, the excess PV energy is exported to the MG.

Case 3. The EV charging demand exceeds the power generated by the RPVS. Under these conditions, the power deficit is supplied by the MG to ensure uninterrupted charging operation.

Case 4. When PV generation is unavailable, the entire EV charging demand is supplied by the MG.

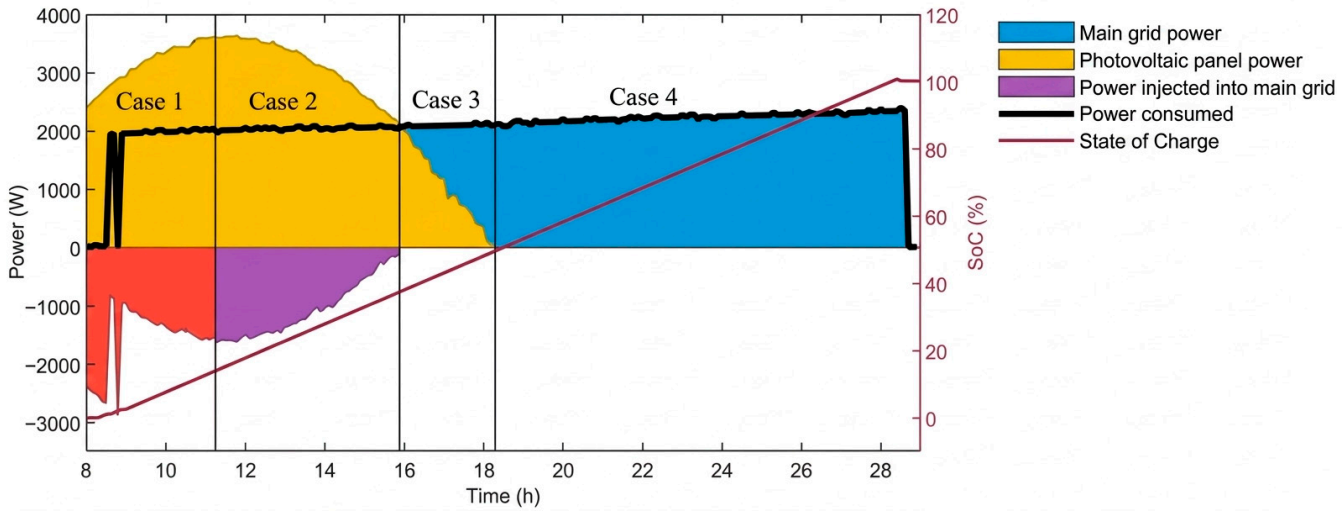


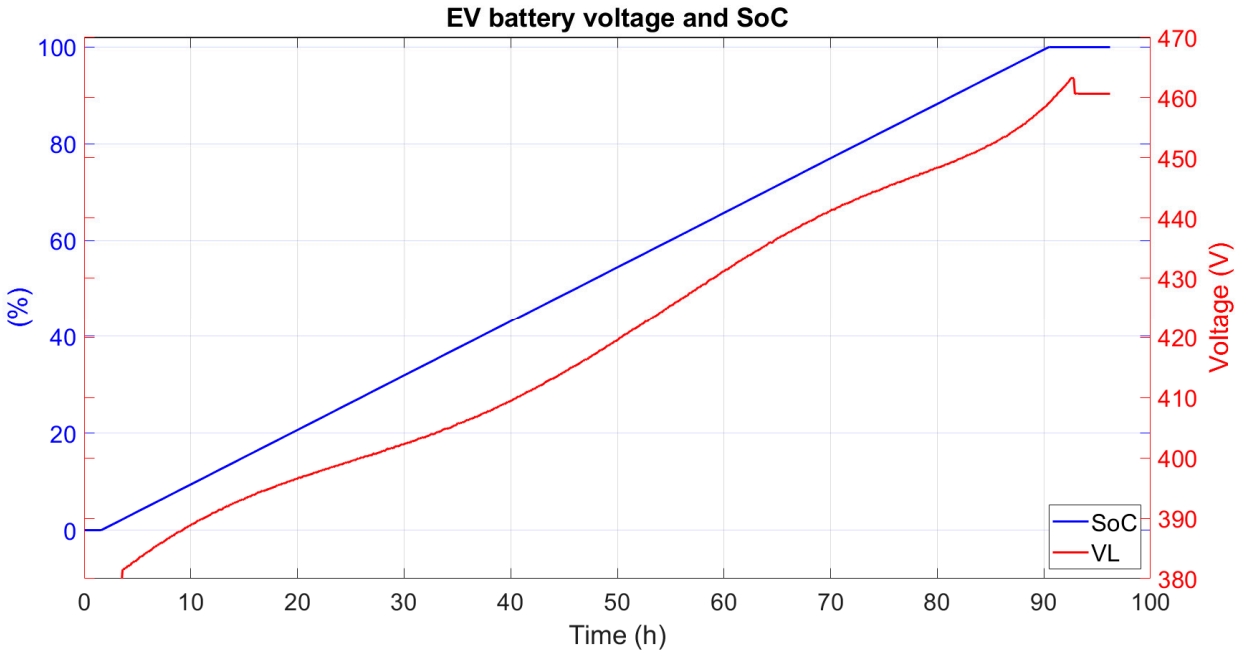
Figure 6. Charging emulation results for the Škoda CITIGOe iV.

4.2. Scenario 1

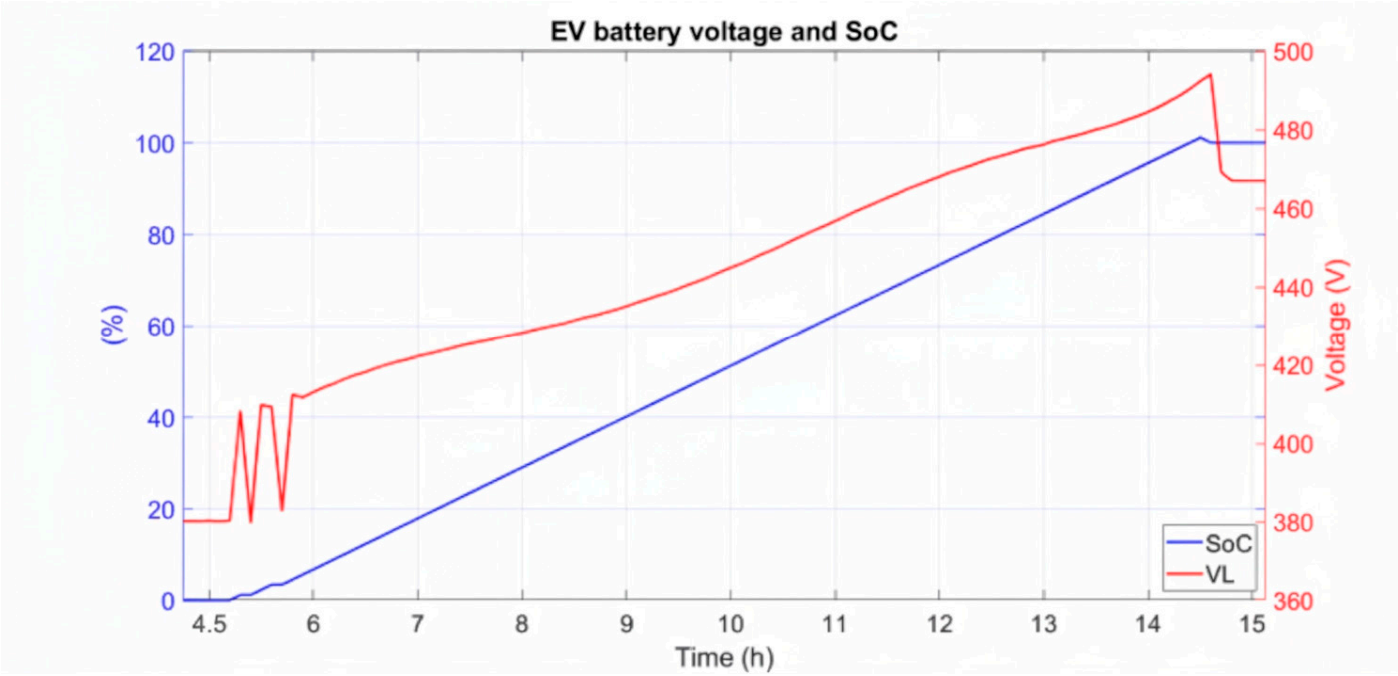
Before executing the emulations, the user configured the operating parameters of both the μG and the EV through the developed HIL platform. For the μG, the efficiencies of the PECs associated with the RPVS $\eta_P = 0.68$ and the ESS $\eta_{(B)} = 0.9216$ were defined, together with the battery charge-discharge efficiency $\eta_{CD} = 0.9$. The ESS was configured using batteries with a nominal voltage of 12 V and a rated capacity of 115 Ah. Furthermore, the residential load demand was set to zero, meaning that the EV represented the only load connected to the μG during all evaluated scenarios. For the EV model, the battery pack of the Tesla Model S was configured using 110 cells connected in series (Ns) and

72 cell strings connected in parallel (Np). The operation of the CES depends on the interaction among the simulated subsystems and the availability of the input data. In all scenarios, the emulation was performed using a sampling interval of 360 s, which was selected according to the available measurement resolution and the time scale of the irradiance and charging datasets.

Figure 7 presents the evolution of the battery SoC and battery voltage during the charging process. The results indicate a total charging time of 88.8 h for charge at Level 1 and 9.5 h for charge at Level 2. Figure 8 illustrates the battery charging power and the power supplied by the MG during the charging process. As expected from the CC charging strategy, the charging power remains approximately constant throughout the charging cycle, resulting in an average power demand of 1.13 kW from the MG for charger Level 1 and 11.156 kWh for charge Level 2. The results show that under CC charging conditions, the EV battery voltage starts at a relatively low value corresponding to an initial SoC of 0%. As the charging process progresses and energy is stored in the battery, the voltage gradually increases until the battery reaches full charge. At the end of the charging process, a slight decrease in the battery voltage can be observed. This behavior is attributed to the equivalent RC battery model employed in the simulation, where part of the stored energy is dissipated through the resistive-capacitive branches that represent polarization effects. The amount of energy stored in these branches depends on the charging current and the dynamic characteristics of the battery model.

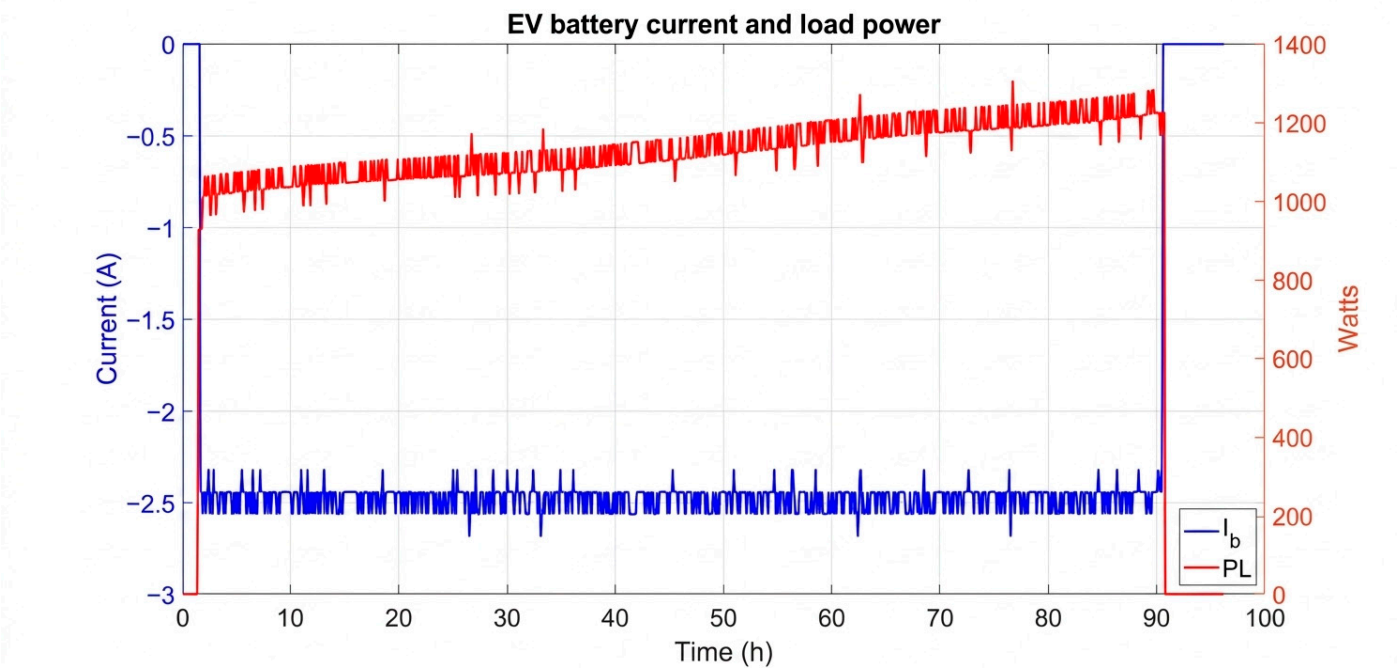


(**a**)

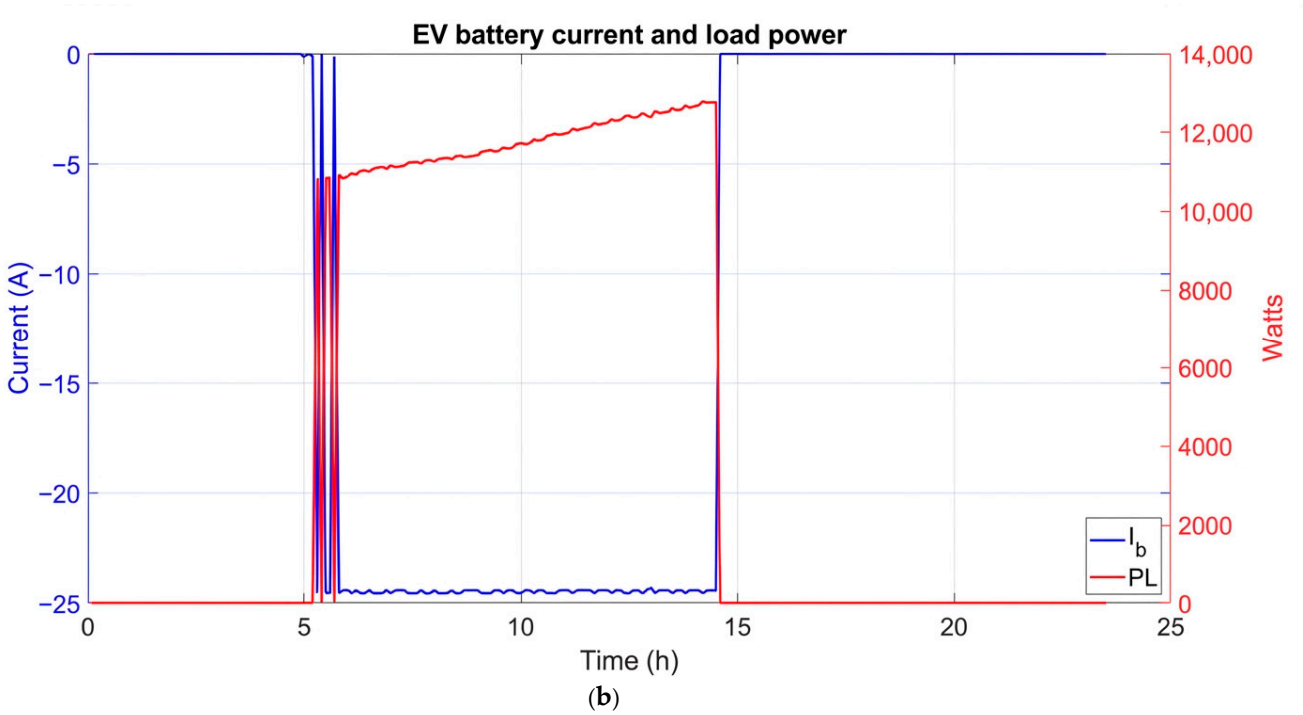


(**b**)

Figure 7. EV battery State of Charge (SoC) and voltage profiles during Scenario 1: (**a**) Charging at Level 1, (**b**) Charging at Level 2.



(**a**)



(**b**)

Figure 8. EV charging power and current demand during Scenario 1: (**a**) Charging at Level 1, (**b**) Charging at Level 2.

4.3. Scenarios 2 and 3

Based on the results obtained from the emulation of Scenario 1, the total energy required to fully charge the EV was 103.198 kWh on average for Scenario 1 Level 1 and Level 2. This value was used as the reference energy demand for the sizing of the RPVS considered in Scenarios 2 and 3. To determine the required size of the RPVS, the daily energy demand of the EV, the Peak Sun Hours (PSH) corresponding to the city of Celaya, Mexico, and a system loss factor were considered. Using these parameters, the required PV generation capacity (Wp), the battery bank capacity (Q), and the required autonomy period in dais (D) were determined using Equations (17) and (18). The resulting sizing methodology ensures that the proposed RPVS is capable of supplying the energy required by the EV charging process while maintaining the operational requirements established for the standalone and MG-connected μG configurations.

$$Wp = Daily\ consumption\ (\text{kWh}) \times loss\ factor\ \div PSH \tag{17}$$

$$Q = \frac{(Daily\ consumption\ (\text{kWh}) \times D)}{Nominal\ voltage\ of\ the\ batteries\ bank} \tag{18}$$

The RPVS was sized to support EV charging using a Level 2 charger under residential operating conditions. For this purpose, the representative daily energy consumption was estimated using the average charging power obtained in Scenario 1. Based on this value, a daily energy demand of 27.12 kWh/day was considered for the sizing process. By considering a system loss factor of 1.17 and 6.17 PSH corresponding to the city of Celaya, Mexico, the required PV generation capacity was calculated as 10 kW. Consequently, the RPVS was configured using 28 PV modules. For the ESS, an autonomy period of two days and a nominal voltage of 96 V were considered. Substituting the corresponding values into Equation (19), a required capacity of 575 Ah was obtained. Since the selected batteries have a rated capacity of 115 Ah, the ESS was configured using five parallel branches, each composed of eight batteries connected in series, thereby meeting the required voltage and capacity specifications. Therefore, the configurations evaluated in Scenarios 2 and 3

consisted of 28 PV modules (Npv), a BB with a nominal capacity of 575 Ah, eight batteries connected in series per branch (NB = 8), and an initial SoC of 80%.

Figure 9 illustrates the power exchange among the components of the proposed CES during the execution of Scenario 2. The green curve represents the power supplied by the ESS, the yellow curve corresponds to the power generated by the RPVS, the red curve indicates the charging power delivered to the ESS, and the black curve represents the EV charging power. When the EV is connected to the μG, four operating conditions can be identified:

Case 1. The energy supplied to the EV is provided exclusively by the ESS of the μG.

Case 2. The energy supplied to the EV is provided jointly by the RPVS and the ESS of the μG.

Case 3. The EV charging demand exceeds the power generated by the RPVS, and neither the ESS nor the system configuration can provide the additional energy required. Therefore, the EMS disconnects the charging process because the ESS does not contain sufficient energy to maintain the requested charging level.

Case 4. Once the EV reaches full charge and the ESS SoC is below 80%, the PV energy generated by the RPVS is redirected to charge the ESS.

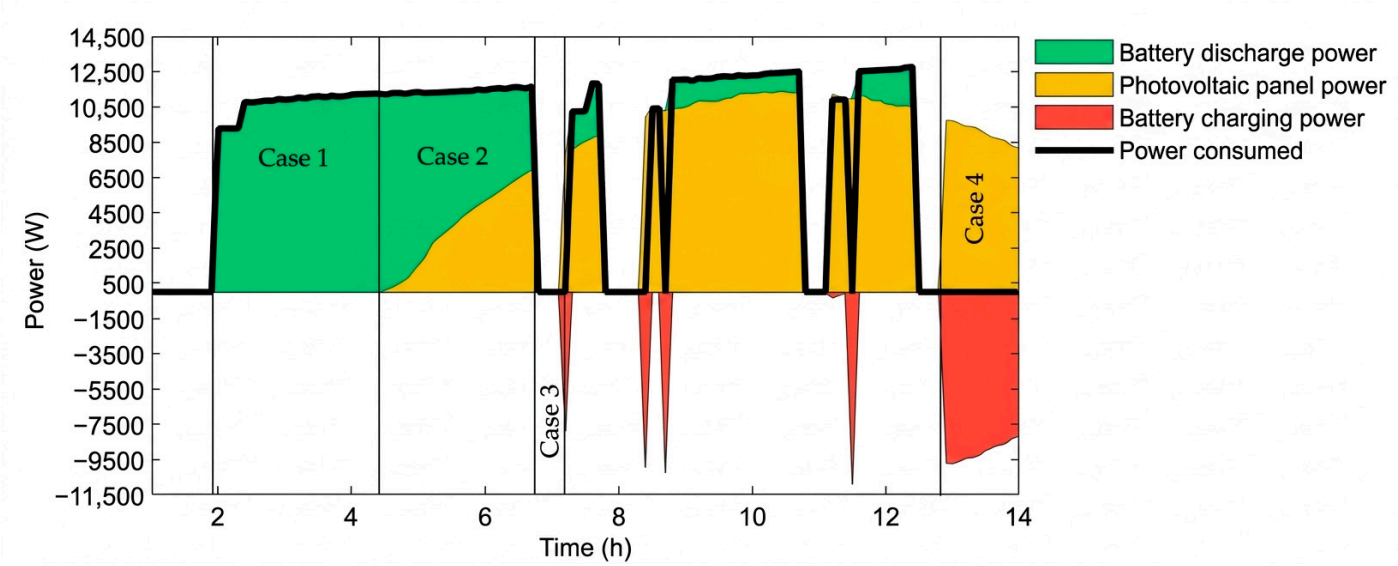


Figure 9. EV charging process in Scenario 2.

Figure 10 shows the evolution of the EV battery SoC and terminal voltage during the emulation process. During the EV charging cycle, several intervals can be observed in which the EMS disconnects the loads and the components of the μG, as described in Case 3. These interruptions affect the overall charging duration. The total charging time was 10.4 h, of which 0.8 h corresponded to system disconnection periods. Therefore, the effective charging time was 9.6 h. The average power required to complete the charging process, considering the entire emulation period, was 9.15 kW. When the disconnection intervals are excluded, the average charging power increases to 10.61 kW. These results demonstrate the influence of energy availability within the isolated μG on the EV charging process. Periods of insufficient energy generation and storage capacity lead to temporary charging interruptions, thereby increasing the total charging time compared to the effective charging period.

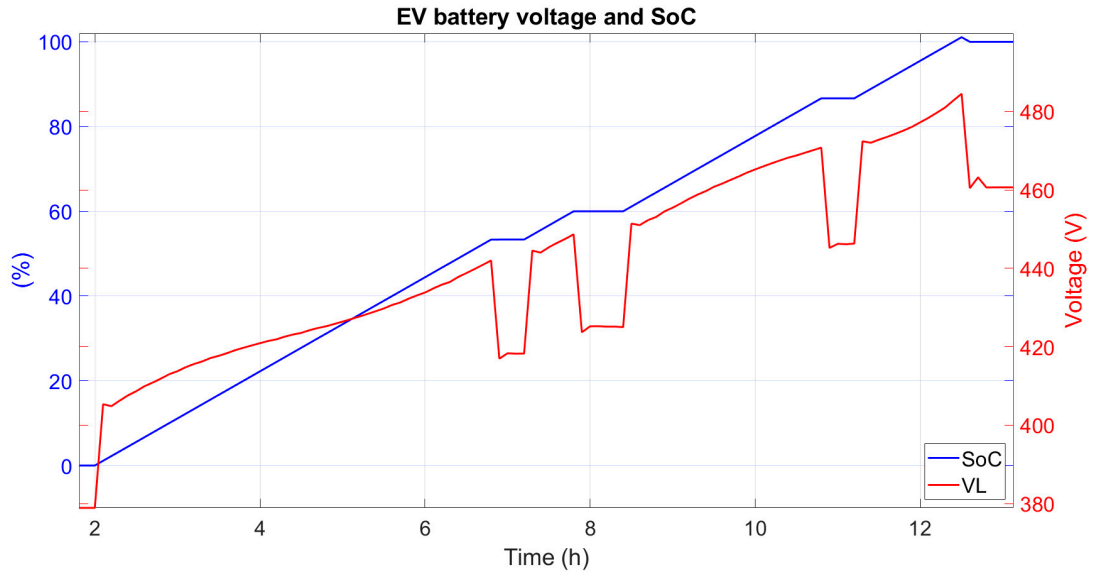


Figure 10. EV battery State of Charge (SoC) and voltage profiles during Scenario 2.

Finally, for the emulation of Scenario 3, the only modification with respect to Scenario 2 was the interconnection of the μG with the MG, while the initial SoC of the ESS was maintained at 80%. Figure 11 illustrates the power exchange among the components of the proposed μG during the EV charging process. The blue curve represents the power supplied by the MG, the purple curve indicates the power exported to the MG, the yellow curve corresponds to the power generated by the RPVS, and the black curve represents the EV charging power.

When the EV is connected to the microgrid, the following operating cases can be identified:

Case 1. The energy supplied to the EV is provided exclusively by the MG.

Case 2. The energy supplied to the EV is jointly provided by the RPVS and the MG.

Case 3. The EV is fully charged, and the SoC of the ESS is greater than or equal to 80%. Therefore, the excess energy generated by the RPVS is exported to the MG.

In this scenario, the EV charging process required a total charging time of 9 h, with an average charging power of 11.6 kW. Figure 12 presents the evolution of the EV battery voltage and SoC during the charging process.

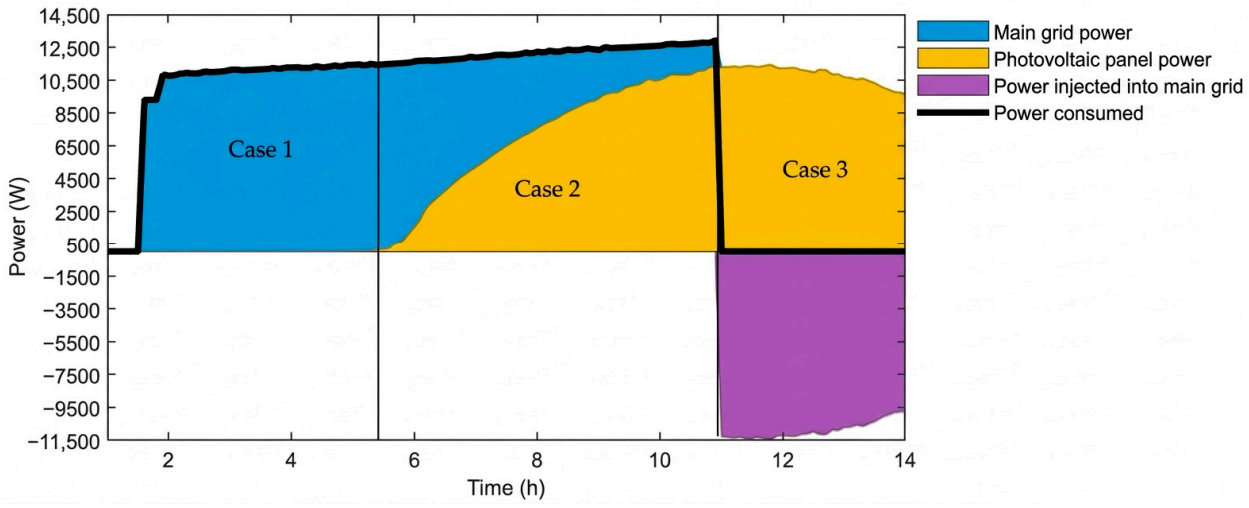


Figure 11. Power exchange between the main grid (MG) and the residential photovoltaic system (RPVS) during Scenario 3.

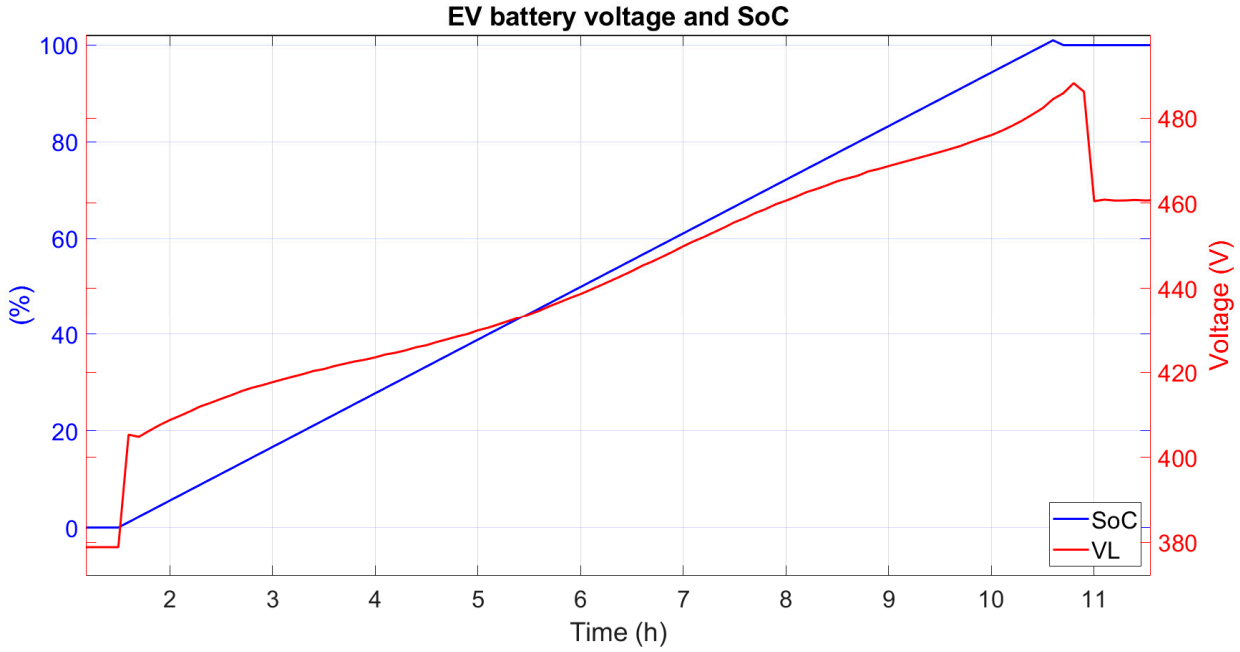


Figure 12. EV battery State of Charge (SoC) and voltage profiles during Scenario 3.

5. Discussion

Based on the results obtained, a comparison was conducted among the three scenarios in terms of energy consumption, average charging power, and charging duration. The corresponding results are summarized in Table 4 where the results from a set of reported experiments are used; it is also worth noting that, for Scenario 2, the values employed correspond to the active time of the charging process and the power delivered during that same period due to disconnection intervals in Scenario 2. The measured energy consumption across the evaluated scenarios was approximately 103.1455 kWh, averaged across the experiments conducted, with a standard deviation of 2.5252 kWh. The observed differences are mainly attributed to the efficiencies considered in each configuration. In Scenario 1, the MG is assumed to supply the required energy without considering transmission and distribution losses between the generation facilities and the residential installation. In contrast, Scenarios 2 and 3 incorporate the efficiencies associated with the RPVS, the PECs, and the ESS, which increase the total energy required to complete the EV charging process.

The charging times obtained in the scenarios with the Level 2 charger differ significantly from those observed in Scenario 1 with the Level 1 charger due to the charging power level employed. Scenario 1 uses a Level 1 charging configuration characterized by a relatively low charging power, resulting in a substantially longer charging time. Conversely, Scenarios that employ Level 2 charging allow significantly higher charging power and consequently reduce the charging duration. Regarding overall performance, Scenario 3 achieved the best results, followed by Scenario 1 with Level 2. Scenario 2 presented the most time spent in scenarios with a Level 2 charger, and, finally, Scenario 1 with a Level 1 charger came last. The superior performance of Scenario 3 is mainly attributed to the combined use of the RPVS and the MG, which provides greater energy availability, reduces charging interruptions, and shortens the total charging time. Although Scenario 2 benefits from the integration of renewable energy, the isolated operation of the μG can lead to temporary charging interruptions when the available PV generation and stored energy are insufficient to satisfy the EV charging demand.

Table 4. Results of the experiments.

Experiment	Energy Consumed (kWh)	Average Charging Power (kW)	Charging Duration (0–100%) (h)
Scenario 1 (Level 1)	100.344	1.13	88.8
Scenario 1 (Level 2)	105.982	11.15	9.5
Scenario 2	101.856	10.61	9.6
Scenario 3	104.4	11.6	9

It is important to note that all evaluated scenarios considered a CC charging strategy. Although Constant Current–Constant Voltage (CC-CV) charging is generally recommended for lithium-ion batteries, the threshold values required for the transition between CC and CV modes may vary depending on battery specifications and battery management strategies. Furthermore, the available reference data does not explicitly indicate whether a CC-CV charging method was employed during the reported charging processes. Consequently, the CC charging strategy was adopted throughout this work to ensure consistency between the reference data and the developed HIL models.

Additionally, the documented charging power corresponds to the power drawn from the AC bus, P_L (see Figure 1), which is supplied to the charger with an assumed efficiency of 0.92, as expressed in Equation (16).

From the perspective of renewable energy utilization, Scenario 2 achieved the highest level of independence from the MG because the EV charging process was supplied exclusively by the RPVS and the ESS. However, the results also demonstrated that the performance of an isolated μG is highly sensitive to the sizing of both the RPVS and the ESS. Although the EV charging process was successfully completed under Level 2 charging conditions, temporary charging interruptions occurred due to periods with insufficient energy availability. These results indicate that maximizing the utilization of PV energy requires an adequate balance among installed PV capacity, ESS energy storage capacity, initial SoC, and local solar resource availability.

To compare the economic and environmental performance of the proposed scenarios, the monthly energy demand associated with EV operation was estimated. According to [48], the average daily distance traveled by passenger vehicles is approximately 49.26 km. Considering that the Tesla Model S Plaid analyzed in this study has a manufacturer-reported energy consumption of 170 Wh/km, a monthly energy requirement of approximately 251.23 kWh was obtained. Under these operating conditions, charging the EV exclusively from the MG may cause the residential user to exceed the limits established by conventional residential tariffs, potentially resulting in reclassification under the DAC tariff. Therefore, a comparative analysis was performed considering the monthly cost of electricity consumption and the associated CO_2 emissions for each charging scenario.

For Scenarios 2 and 3, the energy generated by the RPVS was estimated using the available solar irradiance profile. Environmental effects such as temperature variations, humidity, dust accumulation, and wind speed were not considered. In addition, the irradiance profile was assumed to remain constant throughout the month. Based on the PSH corresponding to Celaya, the installed RPVS capacity, and the efficiencies of the PECs, an average daily PV generation of 41.96 kWh was obtained. Assuming a 30-day month, the resulting monthly PV energy production was estimated as 1258.68 kWh. According to [49], ESSs do not generate direct carbon emissions during charge–discharge operation. Therefore, a specific emission factor of 0 gCO_2/kWh was considered for the ESS operation. For the RPVS, an emission factor of 49.91 gCO_2/kWh was adopted from [50]. This factor includes the life-cycle emissions associated with the manufacture, installation, and operation of the PV generation system and the associated energy storage infrastructure.

From an economic perspective, the Levelized Cost of Energy (LCOE) reported for PV systems with battery storage is approximately $1.044 MXN/kWh [51]. Using this value, the monthly operating costs associated with each charging scenario were estimated.

For Scenario 3, a conservative operating condition was assumed in which the EV is charged primarily during nighttime hours when the RPVS is unable to generate energy. Under this assumption, EV charging is supplied by the MG, whereas the PV energy produced during daytime hours is injected into the MG because the ESS remains fully charged. This represents a less favorable operating condition and provides a conservative estimate of the economic and environmental benefits associated with the proposed system. Based on the estimated monthly energy demand of the EV and the average energy required per charging cycle, approximately 2.43 charging cycles per month would be required. The economic and environmental comparison of the evaluated scenarios is summarized in Table 5; to calculate the cost of MG, Equation 19 based on data presented in Section 3.3 was used, a LCOE of $1.044 MXN/kWh was used to calculate the cost of RPVS, and Equation 13 was used to calculate emissions with corresponding emission factors for MG and RPVS.

$$DAC_{Total} = MC + DAC_{Tarif} \times Energy_{Consumed} \quad (19)$$

where

DAC_{Total}: MG cost

MC: monthly charge ($142.41 MXN for analyzed zone and period)

DAC_{Tarif}: cost per kWh ($6.169MXN for analyzed zone and period)

The cost for a residence under a standard tariff is the same as that presented in Equation (19); for the MC case study, this amounts to $27.75 MXN. The tariffs, which are presented in Section 3.3, are based on net consumption (if this value is less than zero, it is zero).

Table 5. Economic and environmental comparison of the evaluated charging scenarios.

Scenario	Energy Import from MG (kWh)	Energy Export to MG (kWh)	Net Energy from MG (kWh)	MG Cost ($ MXN)	Energy from RPVS (kWh)	RPVS Cost ($ MXN)	Emissions from MG (kg CO_2)	Emissions from RPVS (kg CO_2)	Net Emissions (kg CO_2)	Total Costs ($ MXN)
1	251.23	-	251.23	1692.25	-	-	111.54	-	111.54	1692.25
2	-	-	-	-	251.23	262.28	-	12.53	12.53	262.28
3	251.23	1258.68	−1007.45	27.75	1258.68	1314.06	111.54	62.82	174.36	1340.81

Based on the estimated costs and equivalent CO_2 emissions, the monthly operating cost associated with EV charging reaches approximately $1692.25 MXN in Scenario 1. Scenario 3 presents a lower monthly cost of $1340.81 MXN, while Scenario 2 represents the most economical alternative with an estimated monthly cost of only $262.28 MXN.

From an environmental perspective, Scenario 2 produced the lowest level of emissions, with only 12.53 kgCO_2. Scenario 1 generated 111.54 kgCO_2, whereas Scenario 3 resulted in a total of 174.36 kgCO_2 under the assumptions adopted for the analysis. This result is primarily associated with the consideration of life-cycle emissions attributed to the RPVS and its ESS, as well as the simultaneous use of energy supplied by the MG.

Therefore, Scenario 1 represents the most expensive charging alternative and generates a significant amount of associated emissions. Scenario 2 exhibits the best overall economic and environmental performance, achieving the lowest operating cost and the lowest CO_2 emissions. Scenario 3 reduces the operating cost compared with conventional MG-based charging; however, under the assumptions considered in this study, it exhibits higher equivalent emissions than Scenario 1 due to the adopted life-cycle emission factors.

6. Conclusions

This paper presented the analysis of EV charging using RPVSs through a reconfigurable HIL platform. The proposed platform enabled the real-time evaluation of the dynamic interaction among the residential μG, the ESS, the MG, and the EV under different operating conditions.

The experimental results demonstrated that the developed HIL platform is an effective tool for validating energy management strategies and assessing the technical, economic, and environmental performance of EV charging systems. The platform provided sufficient flexibility to modify PV generation capacity, battery storage capacity, irradiance profiles, and charging conditions, allowing the evaluation of multiple operating scenarios.

A comparative analysis of three charging scenarios was performed. Scenario 1 Level 1, based exclusively on the MG, presented the longest charging time and the highest operating cost. Scenario 2, corresponding to an isolated μG supplied by an RPVS and an ESS, achieved the lowest operating cost and the lowest associated CO_2 emissions. However, its performance was strongly influenced by the availability of solar energy and the stored energy within the ESS. Scenario 3, which combined PV generation with grid support, provided the best operational balance by ensuring charging continuity while increasing the utilization of renewable energy resources.

The results also confirmed the importance of proper sizing of the RPVS and ESS. Insufficient PV generation or storage capacity may lead to charging interruptions and reduced system performance, particularly under isolated operating conditions. Consequently, the sizing of the generation and storage subsystems plays a critical role in guaranteeing reliable EV charging.

The developed HIL platform enables the testing of various EV charging strategies, without being restricted to specific charging protocols or connectors (such as J1772). Furthermore, it allows for specialized testing using actual irradiance data, which can be sourced from environmental monitoring stations to emulate real-world power generation conditions over timeframes ranging from seconds to hours, days, months, or even years.

Additionally, due to the nature of the proposed EMS, the management of the ESS is independent of the specific battery bank technology used, as the system accounts for operational SoC limits tailored to the particular ESS in place. Parameters such as capacity (Q) and nominal voltage can be adjusted within the platform. The integration of the EV's battery bank also facilitates testing with residential loads based on real world data. While the current setup is limited to lithium-ion batteries, it can serve as a benchmark for comparing charging performance against other types of EV battery technologies.

These results may be affected by variations in the timing of the EV charging connection. Furthermore, since inverters are not modeled, the scope is limited to determining the system's energy exchange; analyzing the effects on the MG would require the inclusion of models for each type of charging equipment used.

The validation results were compared against data reported in the literature. Specifically, better performance was achieved for the CITIGOe iV EV, as the charging process reported in [12] was replicated. In contrast, while the theoretical charging time and power capacity for the Tesla Model S are known, no actual data were available for comparison.

From an environmental perspective, the integration of PV generation into residential EV charging infrastructure contributes to reducing dependence on conventional MG electricity and supports the decarbonization of the transportation sector. Furthermore, the proposed energy management strategy successfully prioritized the utilization of renewable energy while maintaining the operational stability of the μG.

Future work will focus on the optimal sizing of PV and ESS, the implementation of advanced intelligent charging, energy management algorithms, and the incorporation of real residential consumption profiles into the HIL platform. Additionally, future

developments will include V2H and V2G operating modes, allowing the evaluation of bidirectional power flow, EV battery utilization, and their impact on μG operation and energy sustainability. In addition, it includes the discharging process to complement the charging behavior by accounting for the power demand generated by the discharging of this type of EV.

Author Contributions: Conceptualization, V.S.-O. and J.M.-N.; methodology, V.S.-O. and A.I.B.-G.; software, E.L.-M. and V.S.-O.; validation, J.M.-N., E.L.-M., and A.I.B.-G.; formal analysis, E.L.-M.; investigation, R.L.-P.; resources, A.R.-S.; data curation, E.L.-M. and R.L.-P.; writing—original draft preparation, J.M.-N.; writing—review and editing, A.R.-S. All authors have read and agreed to the published version of the manuscript.

Funding: This research received no external funding.

Data Availability Statement: The original contributions presented in the study are included in the article; further inquiries can be directed to the corresponding authors.

Acknowledgments: The authors would like to thank the Tecnológico Nacional de México en Celaya (TecNM Celaya) and SECIHTI for their support of this research.

Conflicts of Interest: The authors declare no conflicts of interest.

Abbreviations

The following abbreviations are used in this manuscript:

GHG	Greenhouse gas
COP	Climate Change Conference
BAU	Business-as-Usual
MG	Main grid
V2G	Vehicle-to-Grid
ESSs	Energy storage systems
V2H	Vehicle-to-Home
V2V	Vehicle-to-Vehicle
V2X	Vehicle-to-Everything
DERs	Distributed energy resources
EVs	Electric vehicles
RESs	Renewable energy sources
PV	Photovoltaic
NEDC	New European Driving Cycle
WLTP	Worldwide Harmonized Light Vehicles Test Procedure
EPA	Environmental Protection Agency
MPPT	Maximum Power Point Tracking
PECs	Power electronic converters
RPVSs	Residential photovoltaic systems
μGs	Hybrid microgrids
ESSs	Energy storage systems
EMSs	Energy Management Systems
DC	Direct current
G2V	Grid-to-Vehicle
CC	Constant current
CV	Constant voltage
BBs	Battery Banks
HIL	Hardware-in-the-Loop
PI	Proportional-integral
SAE	Society of Automotive Engineers
IEC	International Electrotechnical Commission

CC-CV	Constant Current–Constant Voltage
VI	Virtual Instrument
GUI	Graphical user interface
G	Irradiance
CES	Charging Emulation System
VCM	Voltage Control Mode
SoC	State of Charge
CFE	Federal Electricity Commission
PSH	Peak Sun Hours
$P_{PV}\|_{DC}$	Photovoltaic power generated in DC
C_{PV}	Nominal power of the RPVS (W)
f_{PV}	Aging factor
G_T	Solar irradiance incident on the PV array (W/m²).
$G_{T,STC}$	Solar irradiance under STC, equal to 1000 W/m².
$\propto_P$	Temperature coefficient of power (%/°C)
T_C	PV cell temperature (°C).
$T_{C,STC}$	PV cell temperature under STC, equal to 25 °C
P_{PV}	Photovoltaic power in AC bus
η_P	Efficiency of PECs used to PV conversion
N_{PV}	Quantity of PV modules used
SoC_0	Initial State of Charge
η_{CD}	Charge/discharge efficiency of BB
i_b	Current of BB
Q	Battery capacity (Ah)
Voc	Open circuit voltage
$\eta(b)$	Efficiency of BB PECs
f	Representation of BB efficiency for charge/discharge
P_G	Main grid power
P_L	Load power
P_B	Battery bank power
VL	Terminal voltage of battery cells
R_1	Resistor of branch RC 1
C_1	Capacitance of branch RC 1
RC_1	Branch RC 1
V_{RC_1}	Voltage of branch RC 1
R_2	Resistor of branch RC 2
C_2	Capacitance of branch RC 2
RC_2	Branch RC 2
V_{RC_2}	Voltage of branch RC 2
Q_T	Total capacity of battery bank
N_P	Number in parallel
N_S	Number in series
V_T	Total voltage
CFE	Comision federal de electricidad
F_E	Emission factor
E_{CO_2}	Emissions of CO_2 (kg CO_2)
E_P	Electrical energy consumption (kWh)
I_{Req}	Required current to charge vehicle
$\%C$	Fraction of total capacity
I_{Ext}	Extracted current
P_{EV}	Power consumption of electric vehicle
$\eta_{CD}(b)$	Charger efficiency
Wp	PV generation capacity
D	Days of autonomy
LCOE	Levelized cost of energy

https://doi.org/10.3390/jlpea16040055

Npv Number of photovoltaic modules

References

1. United Nations. What is the Kyoto Protocol? Available Online: https://unfccc.int/es/kyoto_protocol (accessed on 25 November 2025).
2. United Nations. The Paris Agreement. Available online: https://www.un.org/es/climatechange/paris-agreement (accessed on 15 October 2025).
3. Ritchie, H. Sector by Sector: Where Do Global Greenhouse Gas Emissions Come from? 2020. Available Online: https://ourworldindata.org/ghg-emissions-by-sector (accessed on 31 August 2024).
4. Ritchie, H.; Rosado, P.; Roser, M. CO_2 and Greenhouse Gas Emissions. Available Online: https://ourworldindata.org/co2-and-greenhouse-gas-emissions (accessed on 16 November 2023).
5. Palacios, R.; Masera, O.; Ferrari, L.; Canales, D. (2024). *Futuros Energéticos Para México Al 2050. El Camino Para Una Transición Energética Justa Y Sustentable*; Gobierno de México: Ciudad de México, México, 2024.
6. Saraswathi, V.; Ramachandran, V.P. A comprehensive review on charger technologies, types, and charging stations models for electric vehicles. *Heliyon* **2023**, *10*, e38945. https://doi.org/10.1016/J.HELIYON.2024.E38945.
7. Rachid, A.; El Fadil, H.; Gaouzi, K.; Rachid, K.; Lassioui, A.; El Idrissi, Z.; Koundi, M. Electric Vehicle Charging Systems: Comprehensive Review. *Energies* **2023**, *16*, 255. https://doi.org/10.3390/en16010255.
8. Nivas, M.; Naidu, R.K.P.R.; Mishra, D.P.; Salkuti, S.R. Modeling and analysis of solar-powered electric vehicles. *Int. J. Power Electron. Drive Syst.* **2022**, *13*, 480–487.
9. Silva, W.; Torres, E.; Cardenas, E. Effect on the driving range of an electric vehicle when photovoltaic systems are integrated into its bodywork. *IEEE Lat. Am. Trans.* **2026**, *24*, 1021–1034.
10. Awad, M.; Ibrahim, A.M.; Alaas, Z.M.; El-Shahat, A.; Omar, A.I. Design and analysis of an efficient photovoltaic energy-powered electric vehicle charging station using perturb and observe MPPT algorithm. *Front. Energy Res.* **2022**, *10*, 969482. https://doi.org/10.3389/fenrg.2022.969482.
11. Suh, J. Estimation of Photovoltaic Potential of Solar-Powered Electric Vehicle: Case Study of Commuters on Donghae Expressway, Korea. *Appl. Sci.* **2024**, *14*, 6574. https://doi.org/10.3390/app14156574.
12. Cieslik, W.; Szwajca, F.; Golimowski, W.; Berger, A. Experimental analysis of residential photovoltaic (PV) and electric vehicle (EV) systems in terms of annual energy utilization. *Energies* **2021**, *14*, 1085. https://doi.org/10.3390/EN14041085.
13. Qin, C.; Zhang, J.; Pang, S.; Ma, L. A novel event-triggered secondary control strategy for microgrid considering time-varying delay. *Int. J. Electr. Power Energy Syst.* **2024**, *162*, 110255. https://doi.org/10.1016/J.IJEPES.2024.110255.
14. Atawi, I.E.; Hendawi, E.; Zaid, S.A. Analysis and design of a standalone electric vehicle charging station supplied by photovoltaic energy. *Processes* **2021**, *9*, 1246. https://doi.org/10.3390/pr9071246.
15. Güven, A.F.; Göktepe, Y.Ç.; Bajaj, M.; Blazek, V.; Prokop, L. Techno-economic optimization of renewable-integrated electric vehicle charging infrastructure in campus microgrids considering heterogeneous charging behaviors. *Energy Rep.* **2026**, *16*, 1–34. https://doi.org/10.1016/J.EGYR.2026.109557.
16. Islam, I.; Mahbubul, I.M.; Jadin, M.S.; Al Mansur, A.; Alharbi, T. Lead-acid and lithium-ion batteries for electric mobility applications: A comparative review of performance, economics, industry trends, and future outlook. *J. Energy Storage* **2026**, *155*, 121187. https://doi.org/10.1016/j.est.2026.121187.
17. Himabindu, N.; Hampannavar, S.; Deepa, B.; Swapna, M. Analysis of microgrid integrated Photovoltaic (PV) Powered Electric Vehicle Charging Stations (EVCS) under different solar irradiation conditions in India: A way towards sustainable development and growth. *Energy Rep.* **2021**, *7*, 8534–8547. https://doi.org/10.1016/j.egyr.2021.10.103.
18. Nafeh, A.E.-S.A.; Omran, A.E.-F.A.; Elkholy, A.; Yousef, H. Optimal economical sizing of a PV-battery grid-connected system for fast charging station of electric vehicles using modified snake optimization algorithm. *Results Eng.* **2024**, *21*, 101965. https://doi.org/10.1016/j.rineng.2024.101965.
19. Núñez-Gutiérrez, C. Power-Hardware-in-the-Loop Simulation for Applied Science, a Review to Highlight Its Merits and Challenges. *Inventions* **2025**, *10*, 19. https://doi.org/10.3390/inventions10010019.
20. Franco, F.L.; Mandrioli, R.; Ricco, M.; Monteiro, V.; Monteiro, L.F.C.; Afonso, J.L.; Grandi, G. Electric Vehicles Charging Management System for Optimal Exploitation of Photovoltaic Energy Sources Considering Vehicle-to-Vehicle Mode. *Front. Energy Res.* **2021**, *9*, 716389. https://doi.org/10.3389/fenrg.2021.716389.
21. Rotas, R.; Iliadis, P.; Nikolopoulos, N.; Tomboulides, A. Evaluating Synergies between Electric Vehicles and Photovoltaics: A Comparative Study of Urban Environments. *World Electr. Veh. J.* **2024**, *15*, 397. https://doi.org/10.3390/wevj15090397.

22. Nojavan, S.; Pashaei-Didani, H.; Mohammadi, A.; Ahmadi-Nezamabad, H. Energy management concept of AC, DC, and hybrid AC/DC microgrids. In *Risk-Based Energy Management: DC, AC and Hybrid AC-DC Microgrids*; Elsevier: Amsterdam, The Netherlands, 2020; pp. 1–10. https://doi.org/10.1016/B978-0-12-817491-3.00001-5.
23. Motlagh, S.G.; Oladigbolu, J.; Li, L. A review on electric vehicle charging station operation considering market dynamics and grid interaction. *Adv. Appl. Energy* **2025**, *392*, 126058. https://doi.org/10.1016/j.apenergy.2025.126058.
24. Jian, B.; Wang, H. Hardware-in-the-loop real-time validation of fuel cell electric vehicle power system based on multi-stack fuel cell construction. *J. Clean. Prod.* **2021**, *331*, 129807. https://doi.org/10.1016/j.jclepro.2021.129807.
25. Ucer, E.; Kisacikoglu, M.J. Development of a Hardware-in-The-Loop Testbed for a Decentralized, Data-Driven Electric Vehicle Charging Control Algorithm. *IEEE Trans. Ind. Appl.* **2024**, *60*, 6622–6633. https://doi.org/10.1109/TIA.2024.3384480.
26. Mazza, A.; Pons, E.; Bompard, E.; Benedetto, G.; Tosco, P.; Zampolli, M.; Jaboeuf, R. A Power Hardware-In-the-Loop Laboratory Setup to Study the Operation of Bidirectional Electric Vehicles Charging Stations. In *SEST 2022—5th International Conference on Smart Energy Systems and Technologies, Eindhoven, The Netherlands, 5–7 September 2022*; Institute of Electrical and Electronics Engineers Inc.: New York, NY, USA, 2022. https://doi.org/10.1109/SEST53650.2022.9898502.
27. Benedetto, G.; Bompard, E.; Mazza, A.; Pons, E.; Jaboeuf, R.; Tosco, P.; Zampolli, M. Impact of bidirectional EV charging stations on a distribution network: A Power Hardware-In-the-Loop implementation. *Sustain. Energy Grids Netw.* **2023**, *35*, 101106. https://doi.org/10.1016/j.segan.2023.101106.
28. Ilyushin, P.; Volnyi, V.; Suslov, K.; Filippov, S. State-of-the-Art Literature Review of Power Flow Control Methods for Low-Voltage AC and AC-DC Microgrids. *Energies* **2023**, *16*, 3153. https://doi.org/10.3390/en16073153.
29. Eberle, U.; von Helmolt, R. Fuel Cell Electric Vehicles, Battery Electric Vehicles, and their Impact on Energy Storage Technologies: An Overview. In *Electric and Hybrid Vehicles: Power Sources, Models, Sustainability, Infrastructure and the Market*; Elsevier: Amsterdam, The Netherlands, 2010; pp. 227–245. https://doi.org/10.1016/B978-0-444-53565-8.00009-9.
30. Higashitani, T.; Ikegami, T.; Uemichi, A.; Akisawa, A. Evaluation of residential power supply by photovoltaics and electric vehicles. *Renew. Energy* **2021**, *178*, 745–756. https://doi.org/10.1016/j.renene.2021.06.097.
31. Borray, A.F.C.; Garcés, A.; Merino, J.; Torres, E.; Mazón, J. New energy bound-based model for optimal charging of electric vehicles with solar photovoltaic considering low-voltage network's constraints. *Int. J. Electr. Power Energy Syst.* **2021**, *129*, 106862. https://doi.org/10.1016/j.ijepes.2021.106862.
32. SAE J1772_202401; SAE Electric Vehicle and Plug-in Hybrid Electric Vehicle Conductive Charge Coupler. SAE International: Warrendale, PA, USA, 2024.
33. IEC 62196-1:2022; Plugs, socket-outlets, vehicle connectors and vehicle inlets—Conductive charging of electric vehicles – Part 1: General requirements. International Electrotechnical Commission: Geneva, Switzerland, 2022.
34. Arif, S.M.; Lie, T.T.; Seet, B.C.; Ayyadi, S.; Jensen, K. Review of electric vehicle technologies, charging methods, standards and optimization techniques. *Electronics* **2021**, *10*, 1910. https://doi.org/10.3390/electronics10161910.
35. Alfouly, A.; Valderrama-Blavi, H.; El Aroudi, A. Electric Vehicle Charging Technologies: On-Board and Off-Board Chargers, Power Converters, and Grid Impact Analysis. *Energies* **2026**, *19*, 3169. https://doi.org/10.3390/en19133169.
36. EdgarLopezM25. SEC. GitHub Repository. 2026. Available online: https://github.com/EdgarLopezM25/SEC (accessed on 30 October 2026).
37. Senthilkumar, S.; Mohan, V.; Deepa, R.; Nuthal Srinivasan, M.; Senthil Kumar, T.; Thanikanti, S.B.; Prathap, N. A Review on MPPT algorithms for solar PV systems. *Int. J. Res. Granthaalayah* **2023**, *11*, 25–64. https://doi.org/10.29121/granthaalayah.v11.i3.2023.5086.
38. Chinnathambi, N.D.; Nagappan, K.; Samuel, C.R.; Tamilarasu, K. Internet of things-based smart residential building energy management system for a grid-connected solar photovoltaic-powered DC residential building. *Int. J. Energy Res.* **2022**, *46*, 1497–1517. https://doi.org/10.1002/er.7264.
39. Hernández, A.D.A.; Montañez, F.D.J.G.; Mondragón, V.M.J.; Littlewood, E.C. Circuito Equivalente de Thévenin para el Modelado de la Batería de Litio. *Pist. Educ.* **2022**, *43*, 141.
40. Espedal, I.B.; Jinasena, A.; Burheim, O.S.; Lamb, J.J. Current trends for state-of-charge (SoC) estimation in lithium-ion battery electric vehicles. *Energies* **2021**, *14*, 3284. https://doi.org/10.3390/en14113284.
41. Rout, S.; Das, S.; Kumar, K.S.; Dhanamjayulu, C.; Muyeen, S. Advanced battery modeling and State-of-Charge estimation of lithium-ion batteries: A comprehensive review of modeling approaches, parameterization, and operational challenges. *Energy Strategy Rev.* **2026**, *64*, 102192. https://doi.org/10.1016/J.ESR.2026.102192.
42. Mydeen Pitchai, M.A.B. Data driven state of charge estimation for lithium ion batteries: Evaluating the influence of averaged input features using machine learning. *Next Mater.* **2026**, *11*, 101815. https://doi.org/10.1016/J.NXMATE.2026.101815.

43. MATLAB. Battery. Available online: https://la.mathworks.com/help/sps/ref/battery.html (accessed on 31 December 2025).
44. Xia, B.; Zheng, W.; Zhang, R.; Lao, Z.; Sun, Z. A novel observer for lithium-ion battery state of charge estimation in electric vehicles based on a second-order equivalent circuit model. *Energies* **2017**, *10*, 1150. https://doi.org/10.3390/en10081150.
45. EV-Database. Electric Vehicle Database. Available online: https://ev-database.org/ (accessed on 8 December 2025).
46. CFE. Esquema Tarifario Vigente. Available online: https://app.cfe.mx/Aplicaciones/CCFE/Tarifas/TarifasCRECasa/Casa.aspx (accessed on 6 May 2026).
47. Adiguna, S.; Afandi, A.N.; Bagaskoro, M.C. Techno-economic modeling and analysis of a PV EV charged with battery energy storage system (BESS) on Kalimantan Island. *Glob. Energy Interconnect.* **2025**, *8*, 225–239. https://doi.org/10.1016/j.gloei.2025.01.003.
48. Cadengo Ramírez, M.; Casanova Zavala, W.A.; Mendoza Díaz, A. Desarrollo de Metodología Para la Estimación de Los Vehículos-Kilómetro Recorridos Anualmente, a Nivel Nacional. 2018. Available online: https://trid.trb.org/View/1526086 (accessed on 8 December 2025).
49. Hyundai. ¿Los Coches Eléctricos Contaminan? Available online: https://www.hyundai.com/es/es/zonaeco/eco-life/eco-nciencia/coches-electricos-contaminan (accessed on 6 May 2026).
50. Nugent, D.; Sovacool, B.K. Assessing the lifecycle greenhouse gas emissions from solar PV and wind energy: A critical meta-survey. *Energy Policy* **2014**, *65*, 229–244. https://doi.org/10.1016/J.ENPOL.2013.10.048.
51. International Energy Agency. LCOE and Value-Adjusted LCOE for Solar PV Plus Battery Storage, Coal and Natural Gas in Selected Regions in the Stated Policies Scenario 2022–2030. Available online: https://www.iea.org/data-and-statistics/charts/lcoe-and-value-adjusted-lcoe-for-solar-pv-plus-battery-storage-coal-and-natural-gas-in-selected-regions-in-the-stated-policies-scenario-2022-2030 (accessed on 6 May 2026).

Disclaimer/Publisher's Note: The statements, opinions and data contained in all publications are solely those of the individual author(s) and contributor(s) and not of MDPI and/or the editor(s). MDPI and/or the editor(s) disclaim responsibility for any injury to people or property resulting from any ideas, methods, instructions or products referred to in the content.